Supplementary Information Appendix

Computational Modeling of Three-Dimensional ECM-Rigidity Sensing to Guide Directed Cell Migration

Min-Cheol Kim, Yaron R. Silberberg, Rohan Abeyaratne, Roger D. Kamm, and H. Harry Asada

This SI Appendix includes:

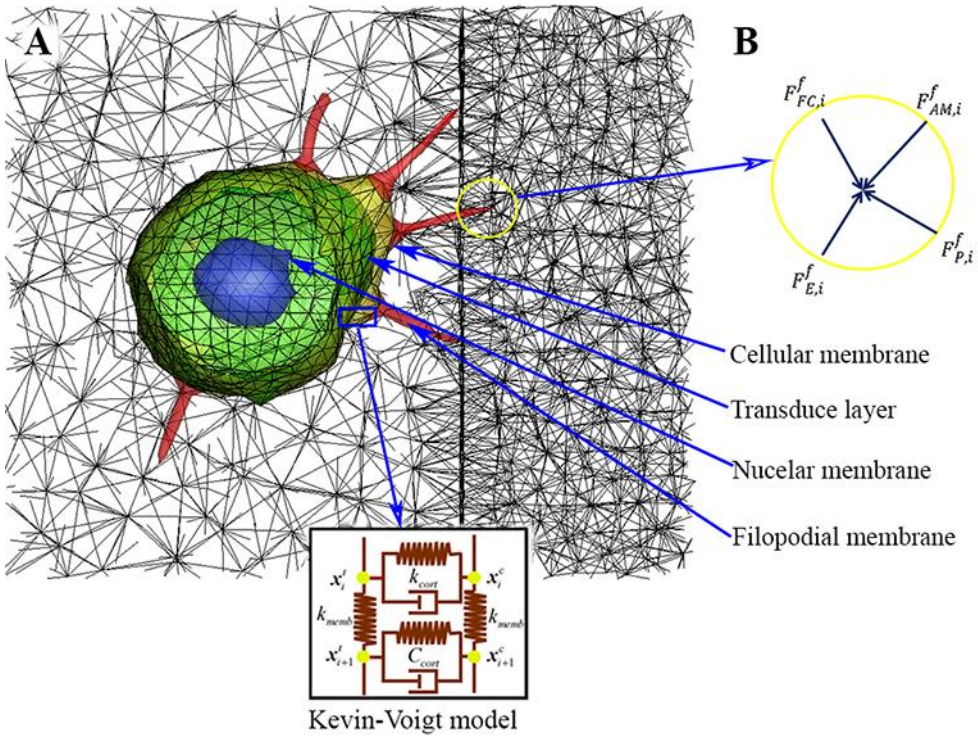

Fig. S1. Dynamic model of cancer cell migration in an elastic ECM fiber network. (**A**) Integrated cancer cell migration model consisting of cellular membrane (yellow), transduce layer (green), nuclear membrane (blue), and filopodial membrane (red). The cellular membrane is not only connected by actin stress fibers (SFs), but also anchored to the elastic substrate by forming focal adhesions (FAs), and viscoelastic behaviors in cellular membrane is modeled using Kelvin-Voigt model. (**B**) The free body diagram of the *i*-th filopodial node in the circle marked in (**A**) where four external forces are acting.

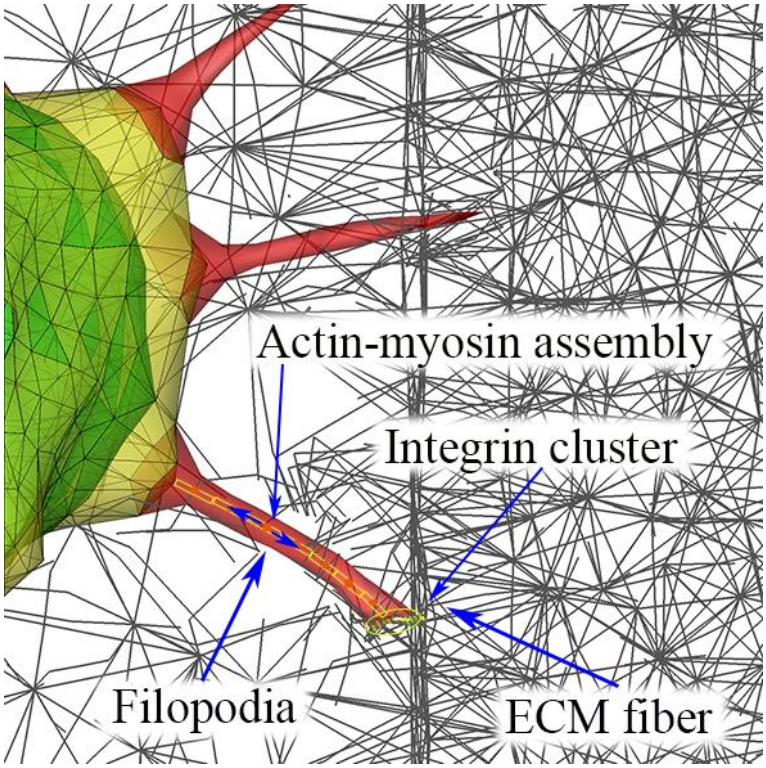

Fig. S2. Mechanical interplay between filopodia and ECM fiber. Schematic showing integrin molecules on the filopodial membrane interacting with an extracellular matrix fiber, and illustrating a stochastic ligand-receptor bonding process at the focal complex site. Also, this schematic shows that filopodia can sense the strength of external force (or the magnitude of $\boldsymbol{F}_{FC,i}^{f}$) from the surrounding ECM fibers, and adjust their myosin sliding rates ($\boldsymbol{v}_m$) with a function of the strength of external force. Contractile actin-myosin assemblies are located along to the shaft of filopodia. Small blue arrows on the actin-myosin assemblies indicate directions of contractile actin filaments, small blue lines are integrin molecules at the tip of filopodium.

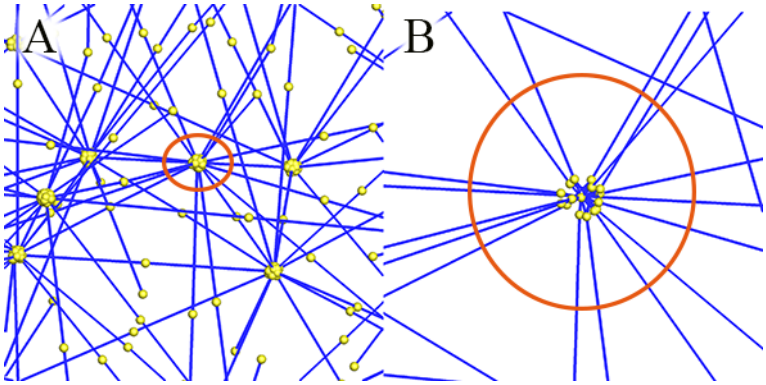

Fig. S3. Composition of ECM fiber network model. (**A**) Segmented ECM fibers were generated between crosslink nodes. Yellow spheres indicate segmented ECM fiber nodes. (**B**) A magnified view in blue circle mark in (**A**) showing examples of three fibers' connectivity with a crosslink node. Blue lines indicated crosslinks between an ECM fiber node and a crosslink node.

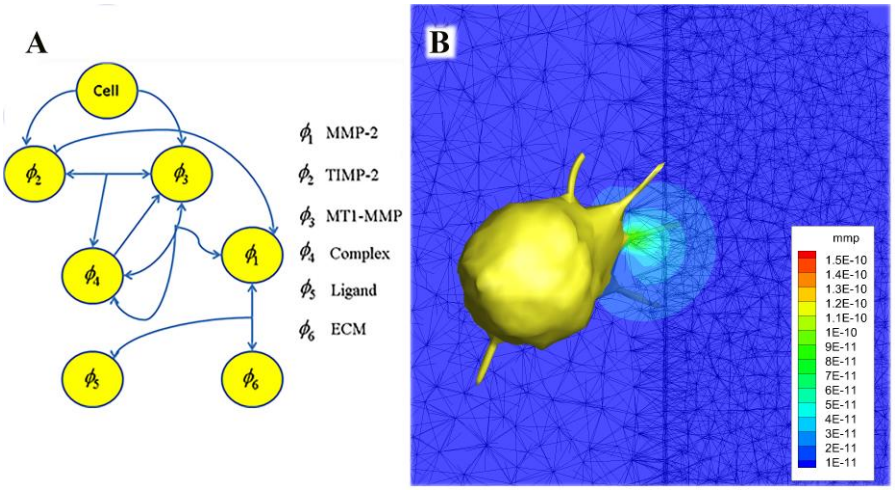

Fig. S4. Schematic diagram of signal pathway. (**A**) The extracellular signal pathway activates MMP-2, and degrades the integrity of ECM. (**B**) An example of simulated results showing MMP-2 concentration contour distribution over ECM fiber network model.

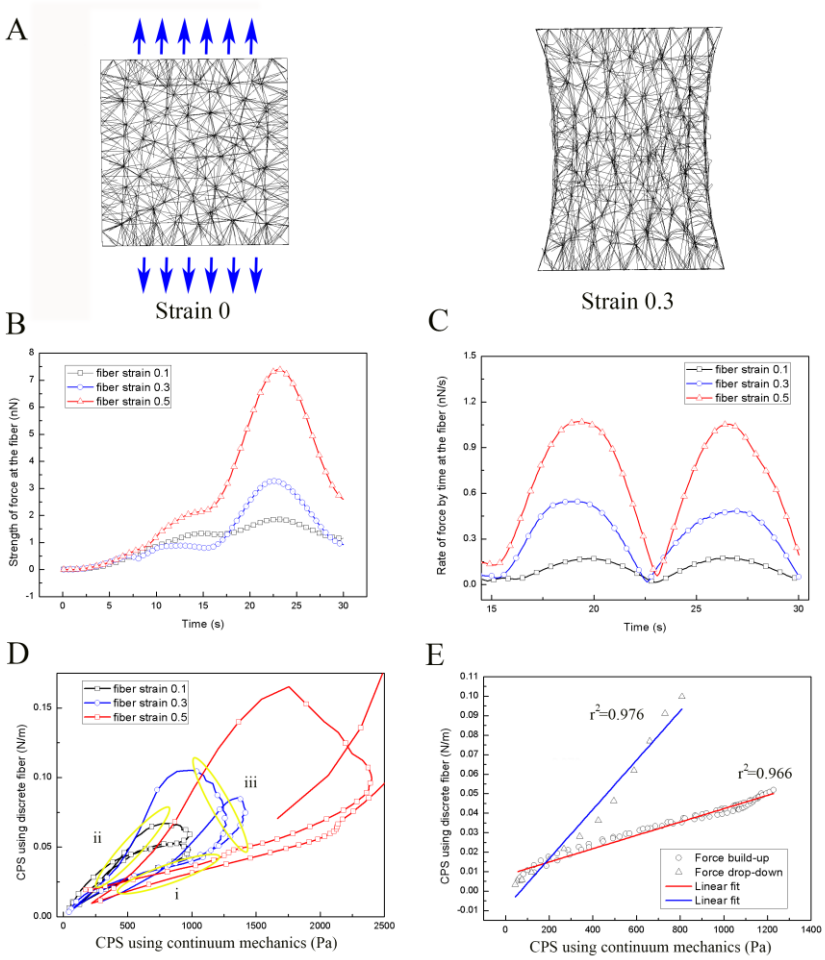

Fig. S5. Simulation of mechanosensing in a soft ECM model. (**A**) Uniaxial tensile force is applied along two different directions in a cubic-shaped soft ECM model with a length of 20 μm for 15 s until the ECM model is strained up to 0.3. Afterwards, a single ECM fiber in the center of ECM model is force to displace to calculate the CPS of surrounding ECM. (**B**) During the event of fiber displacement, the ECM fiber is tensioned during the first period of 7.5 s (from 15 to 22.5 s) and relaxed during the second period of 7.5 s (from 22.5 to 30 s) under three different fiber strains of 0.1, 0.3, and 0.5 (unstressed length of reference fiber is 1 μm). Time-varying applied force curves show maximum values at the time-point of 22.5 when the direction of the force is changed to the opposite direction. (**C**) Rate of applied force by time at the fiber shows three saddle points. (**D**) Characteristic curves of CPSs using continuum mechanics verses CPS using discrete fiber mechanics represent two linear regions (yellow marked i and ii), and one non-linear region (yellow marked iii). (**E**) Selected linear regressions at regions i (r^2 = 0.966) and ii (r^2 = 0.976) between CPS using continuum mechanics and CPS using discrete fiber mechanics in the case of fiber strain 0.3 in (**D**).

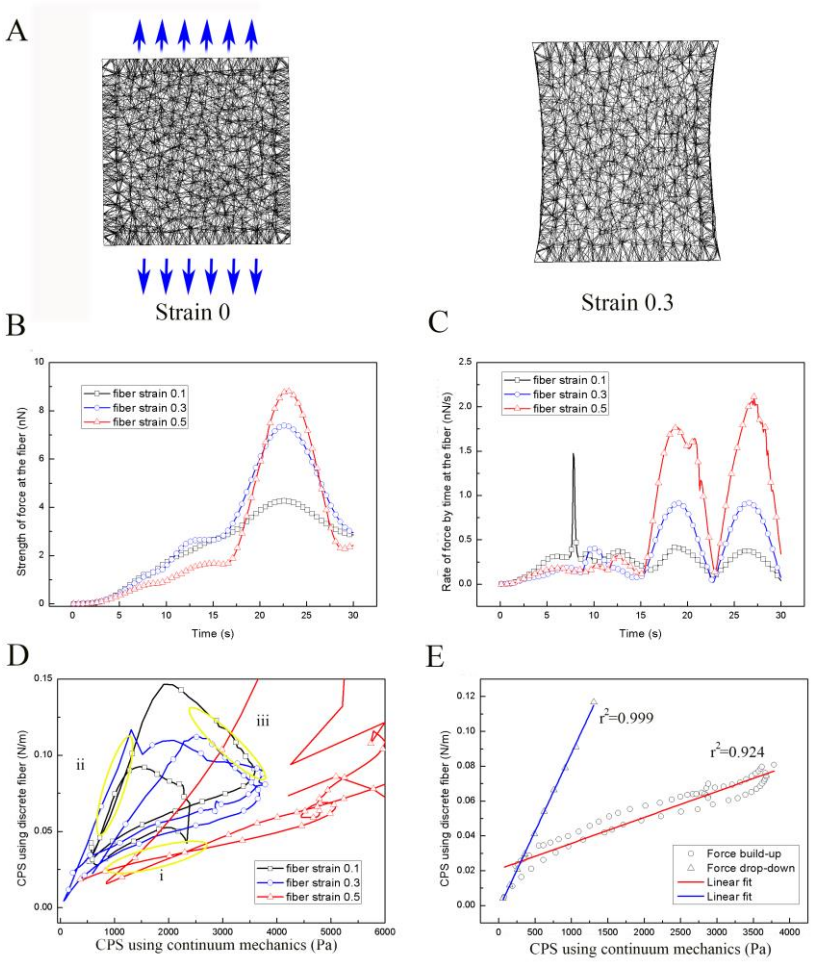

Fig. S6. Simulation of mechanosensing in a stiff ECM model. (**A**) Uniaxial tensile force is applied along two different directions in a cubic-shaped stiff ECM model with a length of 20 μm for 15 s until the ECM model is strained up to 0.3. Afterwards, a single ECM fiber in the center of ECM model is force to displace to calculate the CPS of surrounding ECM. (**B**) During the event of fiber displacement, the ECM fiber is tensioned during the first period of 7.5 s (from 15 to 22.5 s) and relaxed during the second period of 7.5 s (from 22.5 to 30 s) under three different fiber strains of 0.1, 0.3, and 0.5 (unstressed length of reference fiber is 1 μm). Time-varying applied force curves show maximum values at the time-point of 22.5 when the direction of the force is changed to the opposite direction. (**C**) Rate of applied force by time at the fiber shows three saddle points. (**D**) Characteristic curves of CPSs using continuum mechanics verses CPS using discrete fiber mechanics represent two linear regions (yellow marked i and ii), and one non-linear region (yellow marked iii). In particular, regions i and ii are related with the force build-up and the force drop-down, respectively. (**E**) Selected linear regressions at regions i (r^2 = 0.924) and ii (r^2 = 0.999) between CPS using continuum mechanics and CPS using discrete fiber mechanics in the case of fiber strain 0.3 in (**D**).

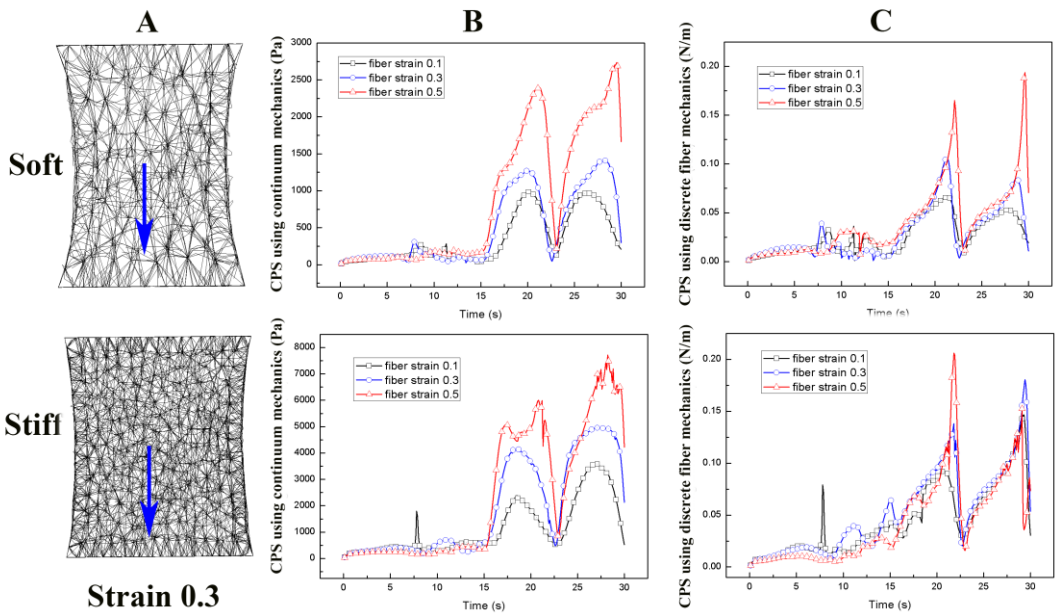

Fig. S7. Characterization of Cell-Probed Stiffness. (**A**) Simulated plots showing that a single ECM fiber in the center of ECM models is forced to displace to calculate two kinds of CPSs of surrounding ECM after both soft and stiff ECM network models are strained up to 0.3. A blue arrow in each ECM model indicates the direction of stretching a single ECM fiber. During the event of fiber displacement, the ECM fiber is tensioned during the first period of 7.5 s (from 15 to 22.5 s) and relaxed during the second period of 7.5 s (from 22.5 to 30 s) under three different fiber strains of 0.1, 0.3, and 0.5 (unstressed length of reference fiber is 1 μm). Graphs show time-varying (**B**) CPS using continuum mechanics, and (**C**) CPS using discrete fiber mechanics for both soft and stiff ECM models.

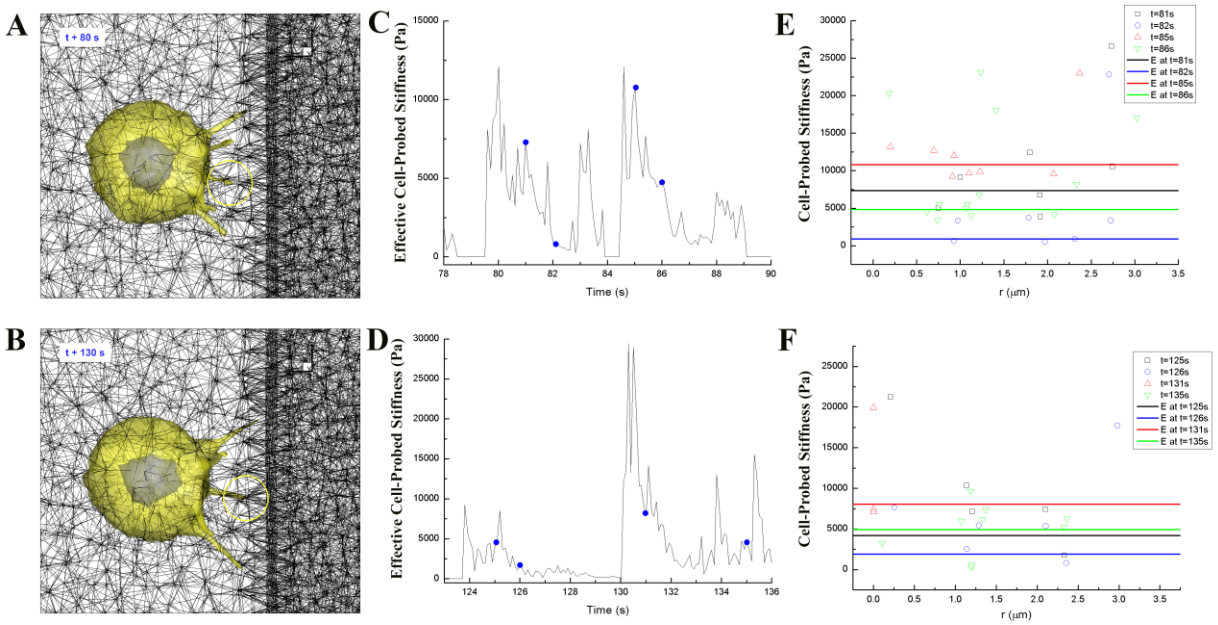

Fig. S8. Mechanosensing of cell interacting with the ECM of varying stiffness. Simulated plots showing cell migration towards stiffer ECM fiber network at two different time points of (**A**) t+80s and (**B**) t+130s. In **(A)**, and (**B)**, yellow shade plots indicate the cellular and filopodia membrane, blue shade plot indicates the nuclear membrane, and black lines are ECM fibers. Time-varying effective Cell-Probed Stiffness (CPS) at the filopodial tip is examined at two time ranges of (**C**) 78~90s and (**D**) 124~136s, and values of effective CPS are found to be higher as the filopodium approaches more towards stiffer ECM. (**E**) and (**F**) Statistical distributions of CPS at selective four time points (blue points in (**C**) and (**D**). Bold lines indicate effective CPS ($\bar{E}^*$), and they are calculated by using Eq. (5). *r* indicates the distance between the tip of filopodia and a node of ECM.

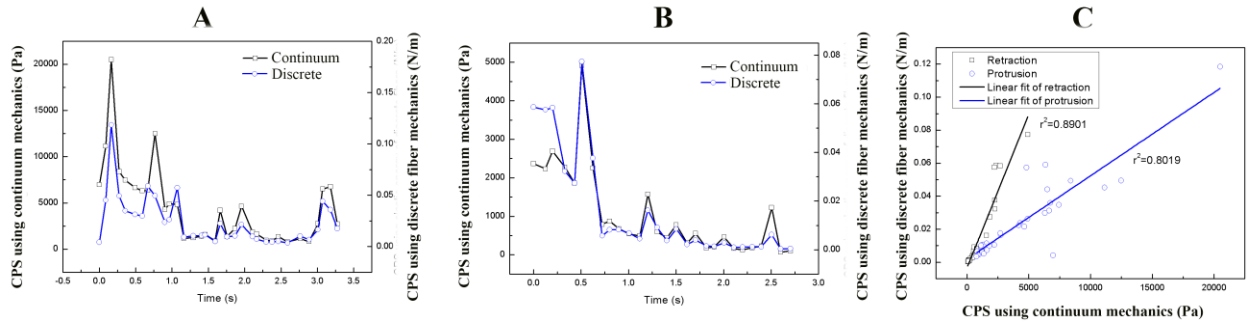

Fig. S9. Comparisons between $\bar{E}^*$ and $\bar{k}_f^*$ at protrusive and retractile phases of filopodia. Graphs showing time-varying CPS for the two methods of continuum mechanics and discrete ECM fibers mechanics at the filopodial (**A**) protrusive and (**B**) retractile phases. (**C**) Linear regressions of protrusive phase (r^2=0.890) and retractile phase (r^2=0.809) between calculated two CPSs in (**A**) and (**B**), respectively.

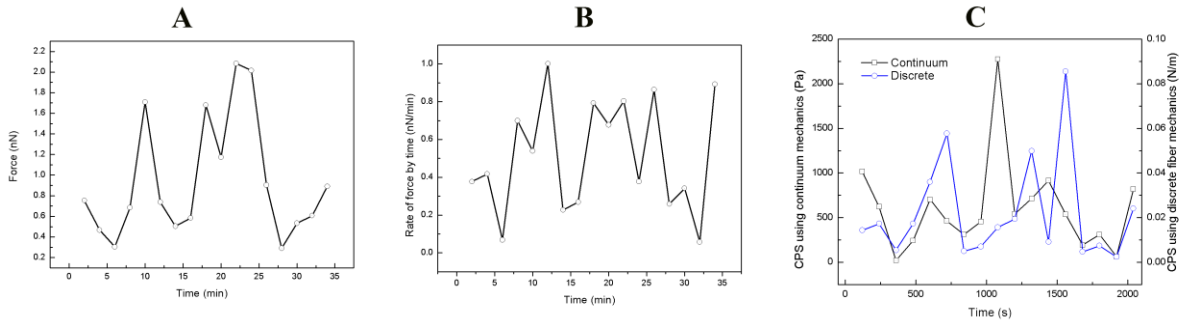

Fig. S10. Experimental observation of filopodial mechanosensing. Time-varying data of (**A**) force, (**B**) rate of force by time, and (**C**) two CPSs using continuum mechanics and discrete fiber mechanics at the filopodia 'b' shown in Fig. 2A and G.

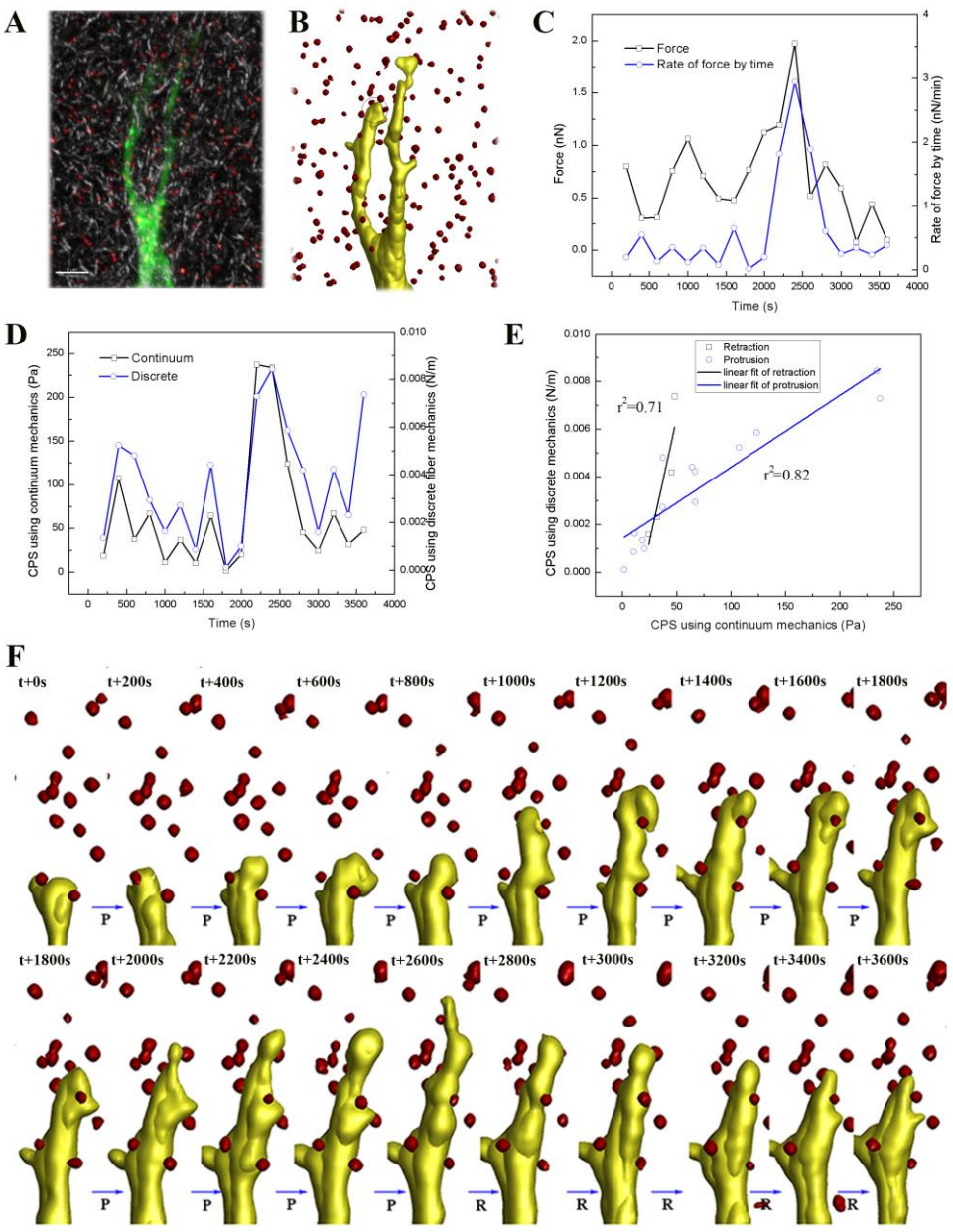

Fig. S11. Experimental measurements of filopodial mechanosensing local ECM stiffness. (**A**) 3D confocal images showing filopodia protrusive and retractile motions in GFP-transfected HUVECs, collagen type 1 fiber network (gray), and fluorescent beads (red). Scale bar = 5 μm. A 3D shade plot in (**B**) indicates 3D reconstructions of filopodia (yellow) and beads (red). Time-varying data of (**C**) force, the rate of force by time, and (**D**) two CPSs using continuum mechanics and discrete fiber mechanics at the filopodia (circle mark in (**B**)). (**E**) Linear regressions of protrusive (r^2=0.82) and retractile phases (r^2=0.71) between calculated two CPSs of the local ECM at filopodium in (**D**), respectively. (F) Series of still shots with time-interval of 200 seconds for 3600 seconds. P and R indicate motion modes of protrusion and retraction, respectively.

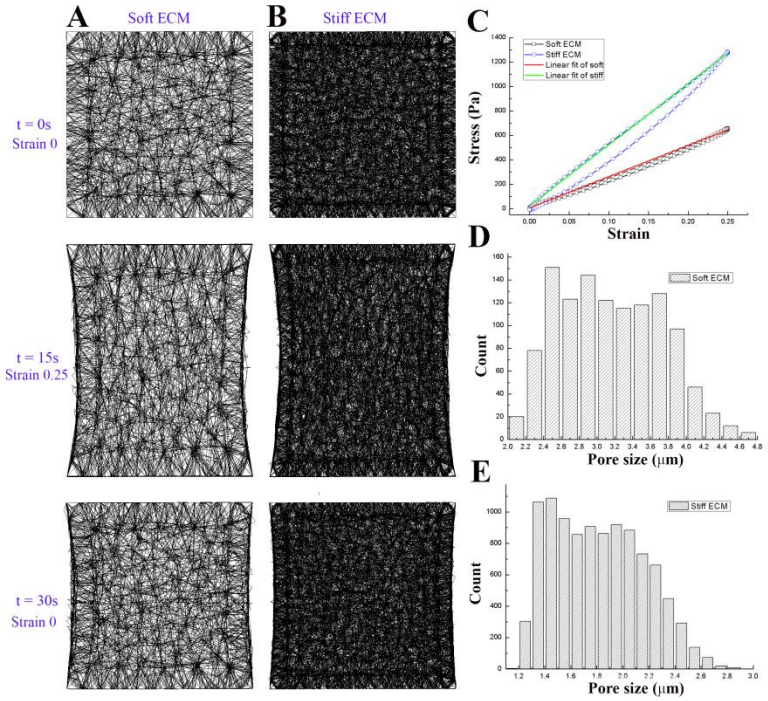

Fig. S12. Simulations of stretching ECM models. Selected examples of deformed ECM network models of (**A**) soft ECM, and (**B**) stiff ECM at three different times of 0, 15, and 30 s, respectively. (**C**) Curves of strain verses stress for soft and stiff ECMs. Slopes of linear fits for soft and stiff ECMs indicate bulk moduli of 2558 and 4999 Pa, respectively. Bar graphs of frequency count for pore sizes of (**D**) soft ECM (3.12±0.57 μm) and (**E**) stiff ECM (1.81±0.34 μm).

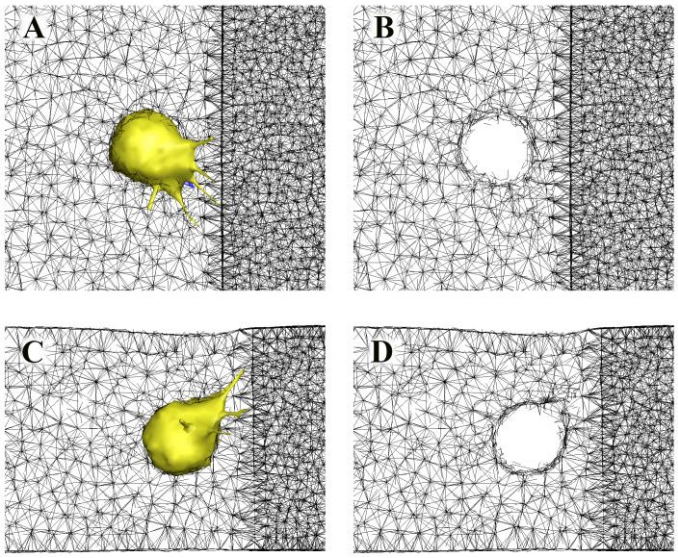

Fig. S13. Volume exclusion effect of the cell. Top view plots of (**A**), and (**B**) show distributions of ECM fibers with the cell, and without the cell, respectively. Side view plots of (**C**), and (**D**) show distributions of ECM fibers with the cell, and without the cell, respectively. Note slice thickness of both plots were set to be 5 μm to visualize the volume exclusion effect of the cell clearly.

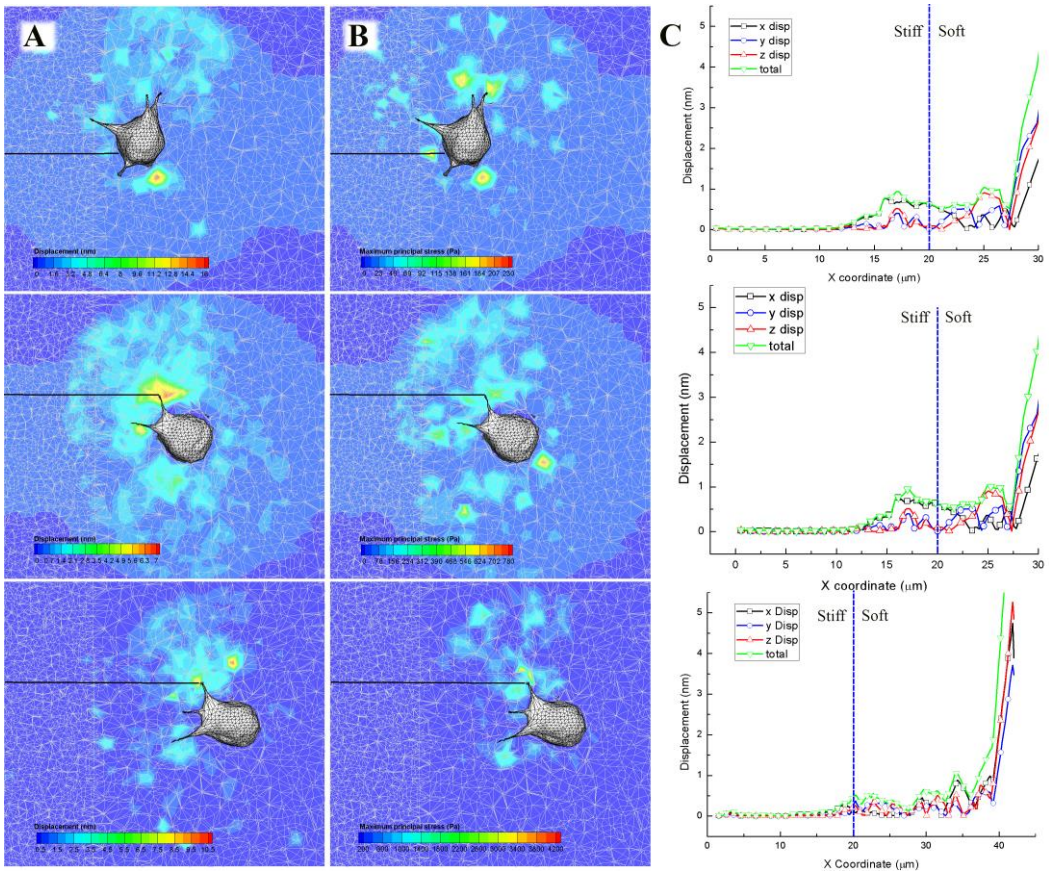

Fig. S14. **Effect of separation distance in directed cell migration towards stiffer ECM**. Selected examples of (**A**) displacement (left panel) and (**B**) maximum principal stress (middle panel) contour slices along both migrating cell and the domain of ECM as a function of separation distance from the surface of the stiffest ECM in which the cell migrates from three different separation distances of 10, 20, and 30 μm. White meshes on the vertical slice indicate ECM fiber network. (**C**) Variations of absolute displacements of x, y, and z directions, and total displacement along to the x coordinate (black lines in (**A**)).

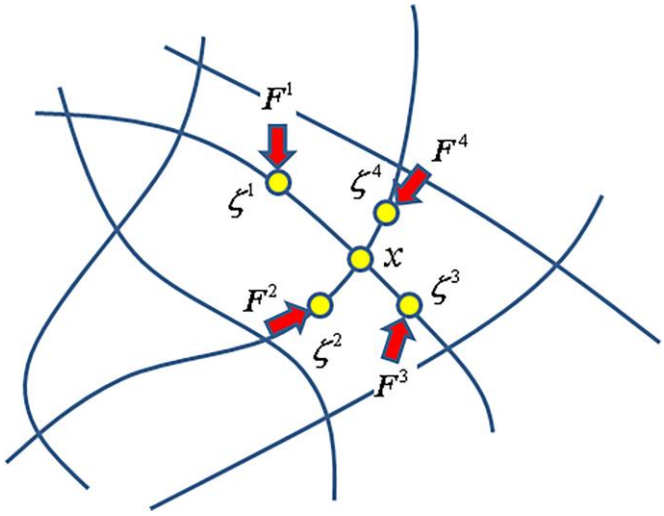

Fig. S15. **Computations of stress tensors at a node of *x*.** The node of x is connected with neighboring nodes of $\zeta^1, \zeta^2, \zeta^3,$ and ζ^4 where forces of $\boldsymbol{F}^1, \boldsymbol{F}^2, \boldsymbol{F}^3,$ and $\boldsymbol{F}^4$ are exerted, respectively. Bold lines, yellow circles, and red arrows indicate ECM fibers, nodes on ECM fibers, and force vectors, respectively.

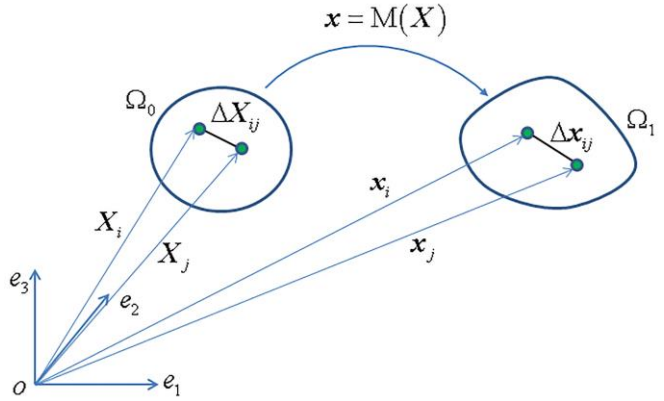

Fig. S16. Motion of a continuum body with discrete ECM fibers. Labels of Boundary Ω_0 and Ω_1 represent discrete ECM fiber system in reference and current configurations, respectively.

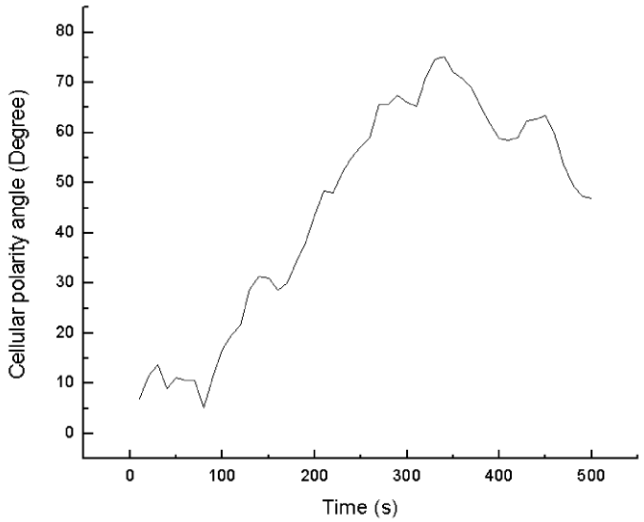

Fig. S17. Time-varying cellular polarity angle. A graph showing temporal variation in cellular polarity angle (PA) during the directed cell migration towards the stiffer ECM shown in Fig. 4.

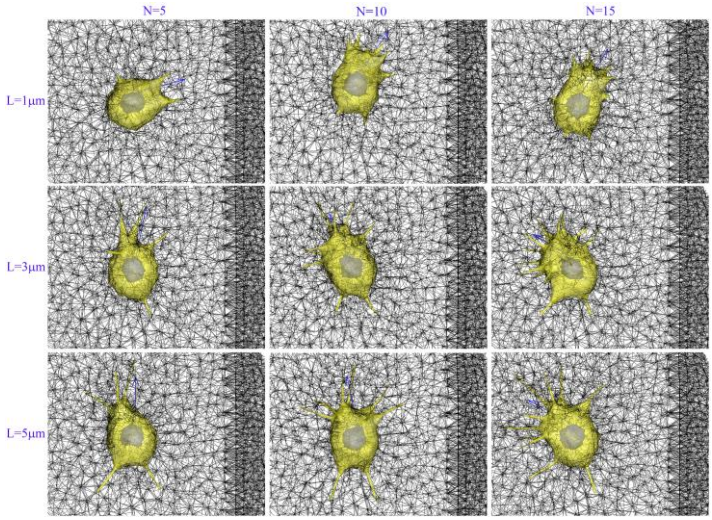

Fig. S18. Cancer cell simulations with numerous and long (or short) filopodia. Selected plots of simulation for the directed cancer cell migration towards the stiffer ECM by tuning filopodial lengths (L) of 1, 3, and 5 μm (rows) and numbers of filopodia (N) of 5, 10, and 15 (columns) at the time-point of 500s. Blue arrow indicates the direction of cellular polarity. Pore sizes of soft (left) and stiff (right) are 3 and 1 μm, respectively. A full image of Fig. 6A.

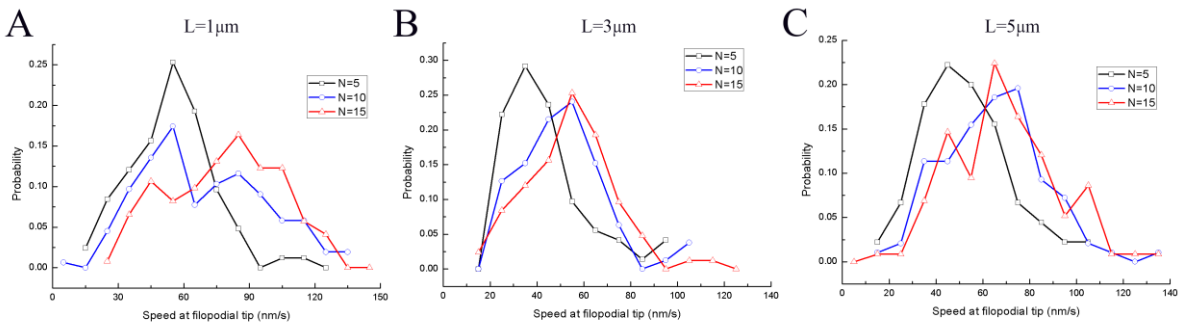

Fig. S19. Probability distributions of the speed at filopodial tip. Graphs show probability distributions of the speed at filopodial tip for nine cases under three different unstressed filopodial lengths of (**A**) 1, (**B**) 3, and (**C**) 5 μm, and three different filopodial numbers of 5, 10, and 15.

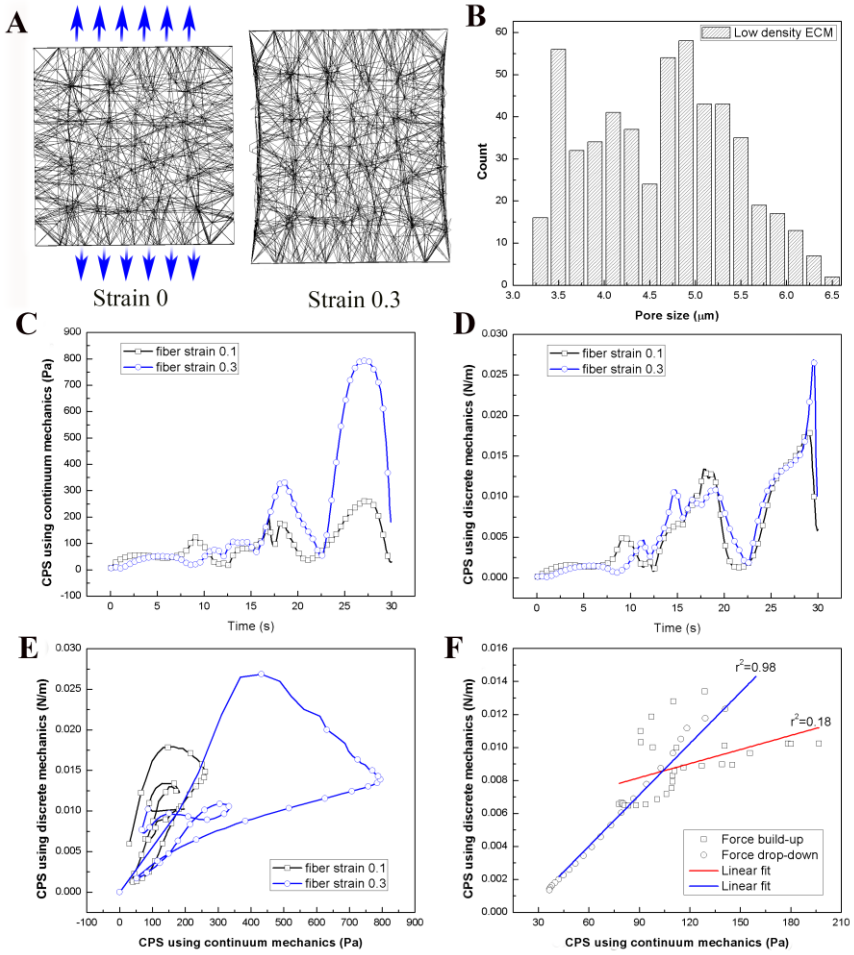

Fig. S20. Simulation of mechanosensing in an ECM model with low fiber density. (**A**) Uniaxial tensile force is applied along two different directions in a cubic-shaped softest ECM model with a length of 20 μm for 15 s until the ECM model is strained up to 0.3. Afterwards, a single ECM fiber in the center of ECM model is force to displace to calculate the CPS of surrounding ECM. (**B**) A bar graph indicates frequency count for pore sizes of softest ECM (4.62±0.77 μm). Graphs show time-varying (**C**) CPS using continuum mechanics, and (**D**) CPS using discrete fiber mechanics for the softest ECM model. (**E**) Characteristic curves of CPSs using continuum mechanics verses CPS using discrete fiber mechanics. Selected linear regressions at regions of force build-up (r^2 = 0.18) and force drop-down (r^2 = 0.98) between CPS using continuum mechanics and CPS using discrete fiber mechanics in the case of fiber strain 0.1 in (**E**).

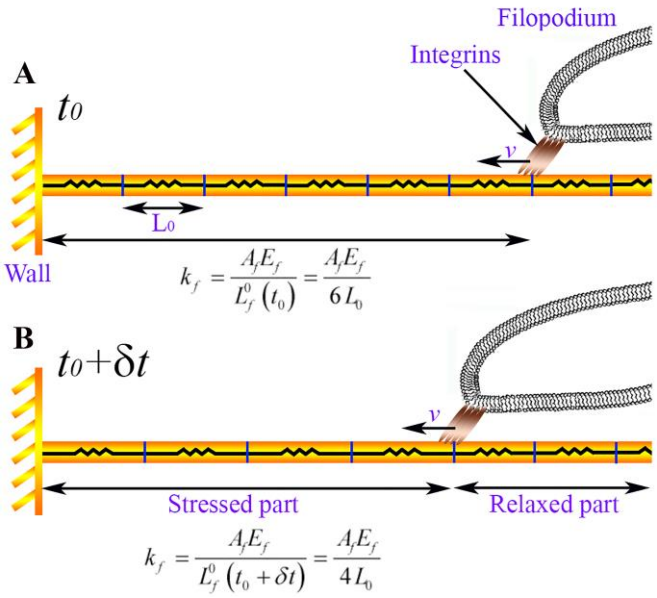

Fig. 21. A schematic showing an increase in effective stiffness (k_f) of a single ECM fiber (consisting of series of elastic springs) during the tugging phase of filopodia dynamics (crawling motion of filopodial tip on the ECM fiber). A) At time of t_0, a tip of filopodium starts tugging on the unstressed single ECM fiber towards the grounded wall. Integrins are clustered on the filopodial tip, and its tip crawls on the unstressed ECM fiber with a sliding rate (v_s). L_0 indicates the unstressed length of one ECM fiber unit, and an integrin clustering is formed on the 6-th ECM fiber unit from the grounded wall. B) At time of $t_0 + \delta t$, the length of stressed part (or the number of ECM fiber units) is reduced more as filopodial tip crawls on the single ECM fiber more towards the left side, but two ECM fiber compartments on the right side become relaxed after the filopodial tugging motion is over.

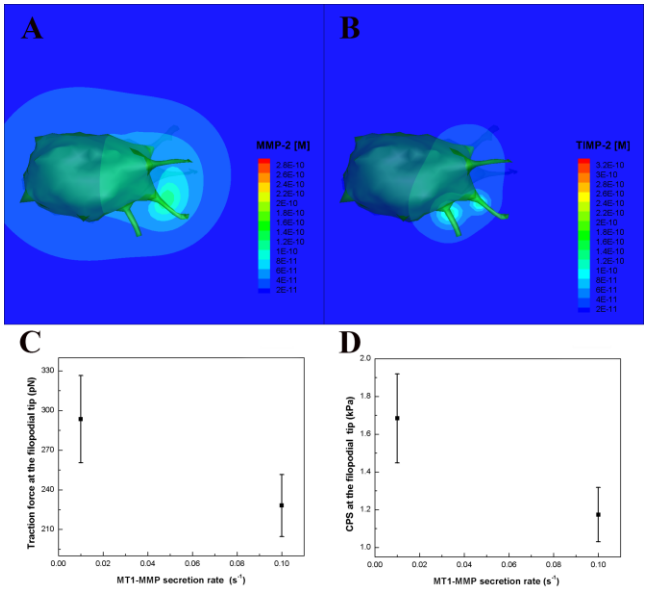

Fig. S22. Cell-Probed Stiffness (CPS) verses MT1-MMP secretion rate. Contour plots of (**A**) MMP-2 and (**B**) TIMP-2 concentration distributions at t = 1200 s using simplified reaction-diffusion model for MMP-2 activation. Variations of (**C**) cellular traction force and (**D**) CPS by interactions between tips of the filopodia and the surrounding local ECM fibers under two different MT1-MMP secretion rates of 0.01 and 0.1 s^{-1}. Error bars indicate standard error of means (n=5).

Table S1. List of simulation parameters.

Parameter	Definition	Value	Sources
A	Area [μm^2]		
A_{AM}	Averaged AMs' cross-sectional area in a filopodium [μm^2]	7.07×10^{-2}	[1]
A_f	Averaged cross-sectional area of a single fiber [μm^2]	$(0.615\sim1.32)\times10^{-3}$	
C_c	Friction coefficients associated with the energy dissipation at the integrin node [N s m^{-1}]	0.001	C
C_{cort}	Drag coefficients associated with viscoelastic behaviors in actin cortex	0.006	C
C_e	Friction coefficients associated with the energy dissipation at the ECM fiber node [N s m^{-1}]	0.001	C
C_f	Friction coefficients associated with the energy dissipation at the filopodial node [N s m^{-1}]	0.001	C
C_t	Friction coefficients associated with the energy dissipation at the transduce node [N s m^{-1}]	0.001	C
C_n	Friction coefficients associated with the energy dissipation at the nuclear node [N s m^{-1}]	0.001	C
F	Force [N]		
$F^f_{P,\max}$	Maximum value of the force due to actin polymerization [nN]	2	C
E_{AM}	Young's modulus value of AMs [kPa]	230	[20]
E^e_f	Young's modulus value of single fiber [MPa]	1	C
H_{AM}	Total elastic energy stored in the AMs in the filopodium [pJ]		
L	Length		
L_b	Stretched length of bonds between receptors and ligands		
$L^1_{AM,i}$	Length of the i-th single unit of AMs at the present time [nm]		
$L^0_{AM,i}$	Length of the i-th single unit of AMs at the previous time [nm]		
L^e_{ij}	Stressed length of the j-th segment of the i-th fiber [μm]		
L^{e0}_{ij}	Unstressed length of the j-th segment of the i-th fiber [μm]		
N_f	Number of nodes at filopodial membrane	60~180	
N_e	Number of nodes at ECM fiber networks	30k~234k	
N_c	Number of nodes at cellular membrane	549	
N_t	Number of nodes at transduce layer	549	
N_n	Number of nodes at nuclear membrane	549	
N^e_i	Number of nodes at the i-th fiber		
N_{AM}	Number of contractile compartments of AM assemblies		
$d_{AM,j}$	Distance of the j-th contractile compartment of AM assemblies [nm]		
h_p	Height from the surface to the i-th integrin node [nm]		
κ_{cort}	Effective spring constant of line elements of the actin cortex [N/m]	8×10^{-3}	C
κ_{LR}	Effective spring constant of ligand-receptor bond [pN/nm]	1.0	[9]
$\kappa_{AM,j}$	Effective spring constant of the j-th AM assemblies in the filopodium [pN/nm]	20.32~33.87	C
$\kappa^e_{f,s}$	The stretching modulus of a fiber [nN]	0.615~1.32	C
$\kappa^e_{f,b}$	The bending modulus of a fiber [pN μm^2]	$(3.02\sim12.81)\times10^{-3}$	C

κ_{memb}	Effective spring constant of line elements of the cell membrane [N/m]	5.0×10^{-5}	[4]
$\theta^{e}_{i\,j}$	Stressed angle at the *j*-th node between two segments in the *i*-th fiber		
$\theta^{e0}_{i\,j}$	Unstressed angle at the *j*-th node between two segments in the *i*-th fiber		
k_{off}	Kinetic dissociation rate [s^{-1}]		
k^{0}_{off}	Kinetic dissociation rate at an unstressed state [s^{-1}]	1	C
n^{k}_{b}	Number of bonds between integrins and ligands at the *k*-th filopodial node		
$\hat{n}^{f}_{R,k}$	Unit vector normal to the local surface of the *k*-th filopodial node		
$\hat{n}_{w}$	Unit normal vector at the local surface of the fiber		
t	Time [s]		
$\hat{\boldsymbol{t}}_{i,k}$	Tangential unit vector at the *k*-th segment in the *i*-th fiber		
$\boldsymbol{v}$	Velocity vector [nm/s]		
v_m	Sliding rate of non-muscle myosin II on the actin filaments [nm/s]		C
v_{m0}	Sliding rate of non-muscle myosin II in the absence of load [nm/s]		
$\boldsymbol{x}$	Location vector [μm]		
$x_{L,i}$	Root of ligand-receptor bonds on the local surface of a fiber [nm]		
x^{e}_{ij}	The *j*-th location vector along to the *i*-th fiber [μm]		
$\boldsymbol{\lambda}$	Equilibrium distance of an integrin [nm]	30	[10]

Sup

c	cytoskeleton
e	extracellular matrix
f	filopodia
n	nucleus
i	*i*-th node
t	transduce layer
0	Previous time or initial state
1	Present time

Sub

AM	Acto-myosin
E	Elastic
FA	Focal adhesion
FC	Focal complex
P	Actin polymerization
SF	Stress fiber
T	Transduce layer
b	bonds
c	cytoskeleton
e	extracellular matrix
f	filopodia
n	nucleus
t	transduce layer

*C means "current work".

Method S1: Computational model for simulating cell invasion into a discrete ECM fiber network

1) Simulation of filopodia penetration dynamics

We assume that filopodia penetration dynamics into 3D ECM consists of four different phases, such as 1) an outgrowing phase due to protrusive actin polymerization (1-3), 2) a retractile phase due to zero or weak focal complex (FC) force at the filopodial tip (4), 3) a contractile phase due to strong FC forces at the filopodial tip, and 4) a tugging phase (filopodial crawling motion on ECM fiber) due to the attachment of a filopodial tip to an nearby ECM (5). Depending on the strength and spatiotemporal properties of the FC formation, the bond of FC at the filopodial tip either ruptures or results in the generation of a significant traction force. This phase plays a critical role in switching among the other phases and coordination of the diverse filopodial dynamics, leading to either success or failure of cell migration depending on local ECM conditions. To solve the filopodia penetration dyanamics into 3D ECM, a dynamic equation at the *i*-th node on the filopodial membrane can be expressed as

$$C_f \frac{d\boldsymbol{x}_i^f}{dt} = \boldsymbol{F}_{E,i}^f + \boldsymbol{F}_{FC,i}^f + \boldsymbol{F}_{P,i}^f + \boldsymbol{F}_{AM,i}^f, \quad i = 1, \cdots, N_f. \tag{S1-1}$$

where C_f is a coefficient of dissipation energy for the filopodial membrane, $\boldsymbol{x}_i^f$ is a position vector at the *i*-th filopodial membrane, and N_f is total number of nodes on the filopodial membrane. $\boldsymbol{F}_{E,i}^f$ is an elastic force at the *i*-th node of the filopodial membrane, and it is obtained by using the virtual work theory in structural mechanics. To this end, the total elastic energy stored in the filopodial membrane is obtained. Two types of total elastic energy are considered. One is the total elastic energy associated with distance changes between the nodes (6, 7):

$$H_L^f = \frac{\kappa_L^f}{2} \sum_{i=1}^{line} \left(L_i^f - L_i^{f0} \right)^2 \tag{S1-2}$$

where L_i^f is the length of the *i*-th line of the filopodial membrane mesh and is updated at every time-step. L_i^{f0} is its relaxed length. κ_L^f is effective stiffness constants of the line elements of the filopodial membrane (5.0×10^{-5} N/m) (8). Similarly, the total elastic energy associated with area changes is given by

$$H_A^f = \frac{\kappa_A^f}{2} \sum_{i=1}^{element} \left(\frac{A_i^f - A_i^{f0}}{A_i^{f0}} \right)^2 A_i^{f0} \tag{S1-3}$$

where A_i^f is the *i*-th mesh area of the filopodial membrane and A_i^{f0} is its relaxed values. κ_A^f is an effective stiffness constant of area elements of the filopodial membrane (1.0×10^{-4} N/m^2) (8). Then, $\boldsymbol{F}_{E,i}^f$ can be obtained by differentiating the two kinds of total energy,

$$\boldsymbol{F}_{E,i}^f = -\kappa_L^f \sum_{i=1}^{line} \left(L_i^f - L_i^{f0} \right) \frac{\partial L_i^f}{\partial \boldsymbol{x}_i^f} - \kappa_A^f \sum_{i=1}^{element} \left(\frac{A_i^f - A_i^{f0}}{A_i^{f0}} \right) \frac{\partial A_i^f}{\partial \boldsymbol{x}_i^f} \ . \tag{S1-4}$$

$\boldsymbol{F}_{FC,i}^f$ is a focal complex force at the *i*-th node of the filopodial membrane, and it is expressed as

$$\boldsymbol{F}_{FC,i}^f = n_{b,i}^f \kappa_{LR} \left(L_b - \lambda \right) \hat{\boldsymbol{n}}_{R,i}^f \tag{S1-5}$$

where $n_{b,i}^{f}$ is the number of integrin-collagen bonds at the *i*-th node of filopodial membrane, κ_{LR} is the spring constant of a single integrin-collagen bond (~1 pN/nm) (9), L_b is the average stretched length of the integrin-collagen bonds, λ is an unstressed length of bonds (~30nm) (10) and $\hat{\boldsymbol{n}}_{R,i}^{f}$ is a unit vector at the local surface of the *i*-th node of filopodial membrane toward the bonding site at the ECM fiber (Fig. S2). Here $\left(L_b-\lambda\right)$ represents the stretched distance from the equilibrium. We utilize Bell's model (11) to incorporate force-dependent reaction rates of $n_{b,i}^{f}$ is expressed in following ordinary differential equation:

$$\frac{dn_{b,i}^{f}}{dt}=k_{on}\left(n_{tot}-n_{b,i}^{f}\right)-k_{off}n_{b,i}^{f} \tag{S1-6}$$

where n_{tot} is total available number of integrin molecules at the *i*-th node of filopodial membrane, k_{on} is the kinetic associate rate for binding integrin molecules and ECM fiber, and it is expressed as (12, 13)

$$k_{on}=k_{on}^{0}\frac{l_{bind}}{Z_0}\exp\left[-\frac{\kappa_{LR}\left(L_b-\lambda\right)^2}{2k_bT}\right] \tag{S1-7}$$

where k_{on}^{0} is the zero forward reaction rate (1 molecule^{-1} s^{-1}), l_{bind} is a binding radius (30 nm) to check whether the *i*-th node of cellular membrane and the node on the fiber are sufficiently close, and k_bT is the unit of thermal energy. Z_0 is the partition function for a integrin molecule confined in a harmonic potential between $-\lambda$ and $L_b-\lambda$, and it is expressed as

$$Z_0=\sqrt{\frac{\pi k_bT}{2\kappa_{LR}}}\left(erf\left[\left(L_b-\lambda\right)\sqrt{\frac{\kappa_{LR}}{2k_bT}}\right]+erf\left[\lambda\sqrt{\frac{\kappa_{LR}}{2k_bT}}\right]\right). \tag{S1-8}$$

k_{off} is the kinetic dissociation rate, and it is known as Bell's equation for the slip bond, which is defined by (11)

$$k_{off}=k_{off}^{0}\exp\left[\frac{\kappa_{LR}\left(L_b-\lambda\right)x_b}{k_bT}\right] \tag{S1-9}$$

where k_{off}^{0} is the zero kinetic dissociation rate in the absent of the force, x_b is the distance between the minimum binding potential and the transition state barrier, and k_bT/x_b represents an intrinsic force ~ 200 pN.

$\boldsymbol{F}_{P,i}^{f}$ is a polymerization force at the tip node of the filopodial membrane, and it is only nonzero nonzero during the outgrowing phase. The polymerization of actin filopodia in a filopodium generate protrusive

force against the membrane of the filopodial tip, and the magnitude of $\boldsymbol{F}_{P,i}^{f}$ is assumed to be ~2 nN since the diameter of filopodium is ~ 300nm consisting of > 30 actin filaments. The direction of $\boldsymbol{F}_{P,i}^{f}$ is assumed to be identical to the direction of normal unit vector at the filopodial root.

$\boldsymbol{F}_{AM,i}^{f}$ is an actin-myosin contractile force at the *i*-th node of the filopodial membrane. The filopodial model is geometrically composed of N_{AM} compartments of actin-myosin (AM) assemblies; the first compartment is attached to the root of filopodium and the last compartment is connected to the tip of filopodium (Fig. S2). We model filopodial contractile motion using AM assemblies as shown in Fig. S2. We assume that the stiffness of an AM is variable as the length of the AM ($L_{AM,j}^{1}$) is decreased by time. Thus, the length of each AM contracts at both ends according to the myosin II sliding rate, and rate of change for $L_{AM,j}^{1}$ is expressed as, $\frac{dL_{AM,j}^{1}}{dt} = -2v_{m,j}$. The stiffness of an AM is expressed as, $\kappa_{AM,j} = \frac{E_{AM}A_{AM}}{L_{AM,j}^{1}}, \quad j = 1..N_{AM}$. Note that $L_{AM,j}^{1}$ is an unstressed length of a single compartment of the *j*-th AM. In addition, to incorporate mechanical interplay between the filopodia and ECM, we adopt the force-velocity relation of muscle myosin II, first proposed by A.V. Hill (14), as following:

$$v_m = v_{m0}\frac{F_{stall} - F_{TR}}{F_{stall} + c_m F_{TR}} \tag{S1-10}$$

where v_{m0} is the sliding rate of myosin in the absence of load, F_{stall} is the stall force of 1 nN, c_m is a dimensionless myosin parameter of 0.1, and F_{TR} is the magnitude of sensed elastic force from the ECM at the tip of filopodium. The total elastic energy stored in the AMs in the filopodium is given by

$$\mathrm{H}_{AM} = \sum_{j=1}^{N_{AM}}\left[\frac{\kappa_{AM,j}}{2}\left(d_{AM,j} - L_{AM,j}^{1}\right)^2\right] \tag{S1-11}$$

where $d_{AM,j}$ represents the distance of the *j*-th contractile AM compartment under tension. Using the virtual work theory, forces due to contractile myosin motor activity at the *j*-th node of filopodial shaft is given by

$$\boldsymbol{F}_{AM,j}^{f} = -\frac{\partial \mathrm{H}_{AM}}{\partial \boldsymbol{x}_{j}^{f}} = -\kappa_{AM,j}\left(d_{AM,j} - L_{AM,j}^{1}\right)\frac{\partial d_{AM,j}}{\partial \boldsymbol{x}_{j}^{f}} + \kappa_{AM,j+1}\left(d_{AM,j+1} - L_{AM,j+1}^{1}\right)\frac{\partial d_{AM,j+1}}{\partial \boldsymbol{x}_{j+1}^{f}}. \tag{S1-12}$$

2) Simulation of intracellular mechanics

The intracellular mechanics is other key mechanisms involved in cell migration in 3D ECM. The essential equations in the model include: 1) an equation for FA dynamics based on Monte-Carlo simulations of ligand-receptor bonds, 2) three equations for deformations of double viscoelastic cellular membranes: an outer cell membrane and an inner transduce membrane, and a nuclear membrane, 3) an equation describing the contractile motion of actin stress fibers, which is extended from FAs on the cortical surface

to the nuclear membrane, and 4) lamellipodium protrusion by actin polymerization (15) with a constant force of 300 pN. The detailed description of the equations in the model can be found in previous works (16, 17). Among them, the major extension in the model of intracellular mechanics presented here is FAs dynamics in 3D ECM fiber network model. The FA force acts between the *i*-th integrin node on the cellular membrane and points of ECM fibers where the extension of the unit vector normal to the cellular membrane interacts with the nearest point of ECM fibers. A dynamic equation at the *i*-th node on the outer cell membrane can be expressed as

$$\left(C_c + C_{cort}\right)\frac{d\boldsymbol{x}_i^c}{dt} - C_{cort}\frac{d\boldsymbol{x}_i^t}{dt} = \boldsymbol{F}_{FA,i}^c + \boldsymbol{F}_{E,i}^c + \boldsymbol{F}_{L,i}^c + \boldsymbol{F}_{T,i}^c, \quad i = 1, \cdots, N_c \tag{S1-13}$$

where C_c and C_{cort} are coefficients of dissipation energy for the outer cell membrane and the actin cortex, respectively. In addition, C_{cort} is a drag coefficient associated with viscoelastic behaviors in the actin cortex. $\boldsymbol{x}_i^c$ is a position vector at the *i*-th node in the cellular membrane, and $\boldsymbol{x}_i^t$ is a position vector at the *i*-th node in the transduce layer. $\boldsymbol{F}_{FA,i}^c$, $\boldsymbol{F}_{E,i}^c$, $\boldsymbol{F}_{L,i}^c$, and $\boldsymbol{F}_{T,i}^c$ are a FA force, an elastic force, a lamellipodium force, and a transduce force representing the elastic force of actin cortex at the *i*-th node of the outer cell membrane, respectively. $\boldsymbol{F}_{FA,i}^c$, can be expressed in a similar manner of focal complex force at the filopodia (See Eq. (S1-5)):

$$\boldsymbol{F}_{FA,i}^c = n_{b,i}^c \kappa_{LR}\left(L_b - \lambda\right)\hat{\boldsymbol{n}}_{R,i}^c. \tag{S1-14}$$

where $n_{b,i}^c$ is the number of integrin-collagen bonds at the *i*-th node of cellular membrane, and $\hat{\boldsymbol{n}}_{R,i}^c$ is a unit vector at the local surface of the *i*-th node of cellular membrane toward the bonding site at the ECM fiber. The elastic force, $\boldsymbol{F}_{E,i}^c$, is also can be similarly expressed like Eq. (S1-4):

$$\boldsymbol{F}_{E,i}^c = -\kappa_L^c \sum_{j=1}^{line}\left(L_j^c - L_j^{c0}\right)\frac{\partial L_j^c}{\partial \boldsymbol{x}_i^c} - \kappa_A^c \sum_{j=1}^{element}\left(\frac{A_j^c - A_j^{c0}}{A_j^{c0}}\right)\frac{\partial A_j^c}{\partial \boldsymbol{x}_i^c}. \tag{S1-15}$$

where L_i^c is the length of the *i*-th line of the cell membrane mesh and is updated at every time-step. L_i^{c0} is its relaxed length. κ_L^c is effective stiffness constants of the line elements of the cell membrane (5.0×10^{-5} N/m) (7, 8). A_i^c is the *i*-th mesh area of the cell membrane and A_i^{c0} is its relaxed values. κ_A^c is an effective stiffness constant of area elements of the cell membrane (1.0×10^{-4} N/m^2) (7). $\boldsymbol{F}_{L,i}^c$ is a characteristic feature at the leading edge of migratory cells. It is believed to be the actual motors which push the cortical cytoskeleton forward during the process of cell migration (18). Normally, cells experience a small protrusive pressure that results from osmotic pressure or actin branches stimulated by activated arp2/3.

Here we assume that the magnitude of the lamellipodium force is constant at 300 pN, and exists at only leading edges of the cell. $\boldsymbol{F}_{T,i}^{c}$ represents the elastic force of actin cortex in the Kelvin-Voigt model (Fig. S1) at the *i*-th node of the outer cell membrane and expressed as

$$\boldsymbol{F}_{T,i}^{c} = -\kappa_{cort}\left(L_{T,i} - L_{T,i}^{0}\right)\frac{\partial L_{T,i}}{\partial \boldsymbol{x}_i^{c}} \tag{S1-16}$$

where κ_{cort} is an effective spring constant of line element of the actin cortex (8.0×10^{-3} N/m), $L_{T,i}$ is the length of the *i*-th line in the actin cortex, and it is updated at every time-step. $L_{T,i}^{0}$ is its relaxed (zero force) length (500 nm).

A dynamic equation at the *i*-th node of the inner transduce membrane can be expressed as

$$-C_{cort}\frac{d\boldsymbol{x}_i^{c}}{dt} + \left(C_t + C_{cort}\right)\frac{d\boldsymbol{x}_i^{t}}{dt} = \boldsymbol{F}_{E,i}^{t} + \boldsymbol{F}_{SF,i}^{t} + \boldsymbol{F}_{T,i}^{t}, \quad i = 1,\cdots,N_t \tag{S1-17}$$

where C_t is a coefficient of dissipation energy for the inner transduce membrane (0.001 Ns/m). $\boldsymbol{F}_{E,i}^{t}$, $\boldsymbol{F}_{SF,i}^{t}$, and $\boldsymbol{F}_{T,i}^{t}$ are an elastic force, an actin stress fiber (SF) force, and a transduce force at the *i*-th node of the inner transduce membrane, respectively. The elastic force, $\boldsymbol{F}_{E,i}^{c}$, is also can be similarly expressed like Eq. (S1-4):

$$\boldsymbol{F}_{E,i}^{t} = -\kappa_L^{c}\sum_{j=1}^{line}\left(L_j^{t} - L_j^{t0}\right)\frac{\partial L_j^{t}}{\partial \boldsymbol{x}_i^{t}} - \kappa_A^{c}\sum_{j=1}^{element}\left(\frac{A_j^{t} - A_j^{t0}}{A_j^{t0}}\right)\frac{\partial A_j^{t}}{\partial \boldsymbol{x}_i^{t}}. \tag{S1-18}$$

where L_i^{t} is the length of the *i*-th line of the transduce layer mesh and is updated at every time-step. L_i^{t0} is its relaxed length. A_i^{t} is the *i*-th mesh area of the cell membrane and A_i^{t0} is its relaxed values.

The actin SF is a bundle of actin microfilaments assembled by actin-myosin II interactions. In the model, the *i*-th node of the inner transduce membrane is connected to the *j*-th node of nuclear membrane by a SF. Its connection to the *j*-th node of nuclear membrane is determined by the nearest distance from the *i*-th node of the inner membrane to the nucleus. The stiffness of a SF is variable. According to the literature, the stiffness increases with a contractile agonist (histamine) and decreases with a relaxing agonist (isoproterenol) (19). These characteristics must be reflected in the formulation of the SF stiffness:

$$\kappa_{SF} = \frac{E_{SF}A_{SF}}{L_{SF,i}^{1}} \tag{S1-19}$$

where E_{SF} is Young's modulus of SFs (230 kPa) directly measured from isolated smooth muscle cells (20), A_{SF} is the average cross-sectional area of SFs (250 nm in radius (21)), and $L_{SF,i}^{1}$ is the length of a single compartment of the *i*-th SF. Similarly, the elastic energy stored in the *i*-th SF is given by

$$E_{SF,i} = \sum_{j=1}^{N_{SF}} \left[\frac{\kappa_{SF}}{2} \left(\frac{d_{SF,i}}{N_{SF}} - L^1_{SF,j} \right)^2 \right]$$
$$= \frac{\kappa_{SF}}{2} \left(\frac{d_{SF,i}}{N_{SF}} - L^1_{SF,1} \right)^2 N_{SF} = \frac{\kappa_{SF}}{2N_{SF}} \left(d_{SF,i} - N_{SF} L^1_{SF,1} \right)^2 \quad \text{(S1-20)}$$

where N_{SF} is the number of contractile compartments in the *i*-th SF, $d_{SF,i}$ represents the distance between *i*-th node of inner membrane and the *j*-th node of nuclear membrane for a SF connected to the nucleus. It should be noted that $d_{SF,i}$ physically means the length of SFs under tension and $L^1_{SF,1}$ represents the length of a single unstressed bundle of SFs. Using the virtual work theory, forces due to actin SFs' motor activity at the *i*-th node of inner membrane and the *j*-th node of nuclear membrane is given by

$$\boldsymbol{F}^t_{SF,i} = -\frac{\partial E_{SF,i}}{\partial \boldsymbol{x}^t_i} = -\frac{\kappa_{SF}}{N_{SF}} \left(d_{SF,i} - N_{SF} L^1_{SF,i} \right) \frac{\partial d_{SF,i}}{\partial \boldsymbol{x}^t_i} \quad \text{(S1-21)}$$

Actin motor activity is assumed not to start until the other end of a SF is connected to the nucleus. The myosin II's sliding rate is known to fluctuate (i.e. is non-uniform) unlike myosin I which slides with a uniform rate. Furthermore, the sliding rate of myosin II is adjusted by sensing the transmitted focal adhesion force from the ECM (22). To incorporate these characteristics into the model, force-velocity relation of muscle myosin II is similarly adopted like Eq. (S1-10). Initially, the length of sarcomere unit is 800 nm ($L^1_{SF,i}$ =800 nm at t=0s), which contracts until 60 % of the initial length has contracted. As the contraction takes place at both sides of each sarcomere unit, the minimum time required for 60 % contraction is calculated as 16 s with v_{m0}. Furthermore, an additional condition for terminating actin motor activity is also considered when integrin nodes are broken from FA formations.

The transduce force, $\boldsymbol{F}^t_{T,i}$,is expressed as

$$\boldsymbol{F}^t_{T,i} = -k_{cort} \left(L_{T,i} - L^0_{T,i} \right) \frac{\partial L_{T,i}}{\partial \boldsymbol{x}^t_i} = -\boldsymbol{F}^c_{T,i} \,. \quad \text{(S1-22)}$$

Lastly, a dynamic equation at the *i*-th node of the nuclear membrane can be expressed as

$$C_n \frac{d\boldsymbol{x}^n_i}{dt} = \boldsymbol{F}^n_{E,i} + \boldsymbol{F}^n_{SF,i}, \quad i = 1, \cdots, N_n \quad \text{(S1-23)}$$

where C_n is a coefficient of dissipation energy for the nuclear membrane (0.001 N s m^{-1}), and $\boldsymbol{x}^n_i$ is a position vector at the *i*-th node in the membrane of nucleus. $\boldsymbol{F}^n_{E,i}$ and $\boldsymbol{F}^n_{SF,i}$ are an elastic force and a SF force at the *i*-th node of the nuclear membrane, respectively. The elastic force, $\boldsymbol{F}^n_{E,i}$, can be expressed in a similar manner of the Eq. (S1-4) as

$$\boldsymbol{F}^n_{E,i} = -\kappa^n_L \sum_{j=1}^{line} \left(L^n_j - L^{n,0}_j \right) \frac{\partial L^n_j}{\partial \boldsymbol{x}^n_i} - \kappa^n_A \sum_{j=1}^{element} \left(\frac{A^n_j - A^{n0}_j}{A^{n0}_j} \right) \frac{\partial A^n_j}{\partial \boldsymbol{x}^n_i} \quad \text{(S1-24)}$$

where L_i^n is the length of the *i*-th line of the nuclear membrane mesh and is updated at every time-step. L_i^{n0} is its relaxed length. κ_L^n is effective stiffness constants of the line elements of the nuclear membrane (5.0×10^{-3} N/m) (23). A_i^n is the *i*-th mesh area of the nuclear membrane and A_i^{n0} is its relaxed values. κ_A^n is an effective stiffness constant of area elements of the nuclear membrane (1.0×10^{-4} N/m^2). The SF force, $\boldsymbol{F}_{SF,i}^n$ at the *i*-th node of the nuclear membrane is expressed as

$$\boldsymbol{F}_{SF,i}^n = -\frac{\partial E_{SF,i}}{\partial \boldsymbol{x}_i^n} = -\frac{\kappa_{SF}}{N_{SF}}\left(d_{SF,i} - N_{SF}L_{SF,i}^1\right)\frac{\partial d_{SF,i}}{\partial \boldsymbol{x}_i^n} = -\boldsymbol{F}_{SF,i}^t \tag{S1-25}$$

In particular, Equations (20) and (24) are coupled with the viscoelastic actin cortex using kelvin-voigt model (a spring and a dashpot together in parallel). To solve these ordinary differential equations numerically, they should be converted with respect to vectors $\left\{\frac{d\boldsymbol{x}_i^c}{dt}, \frac{d\boldsymbol{x}_i^t}{dt}\right\}^T$ as followings:

$$\begin{pmatrix}\frac{d\boldsymbol{x}_i^c}{dt}\\ \frac{d\boldsymbol{x}_i^t}{dt}\end{pmatrix} = \frac{1}{C_cC_t + C_{cort}(C_c+C_t)}\begin{pmatrix}C_t+C_{cort} & C_{cort}\\ C_{cort} & C_c+C_{cort}\end{pmatrix}\begin{pmatrix}\boldsymbol{F}_{FA,i}^c + \boldsymbol{F}_{E,i}^c + \boldsymbol{F}_{L,i}^c + \boldsymbol{F}_{T,i}^c\\ \boldsymbol{F}_{E,i}^t + \boldsymbol{F}_{SF,i}^t + \boldsymbol{F}_{T,i}^t\end{pmatrix} \quad i=1,\cdots,N_c. \tag{S1-26}$$

3) Simulation of discrete ECM fiber mechanics

We assume the ECM fiber network to be composed of elastic ECM fibers and crosslinks, which make strong bonds between adjacent fibers (24). The elastic energy stored in the ECM fiber network can be expressed in terms of the stretching and bending properties of the constituent fibers. The stretching modulus of a fiber is given by $\kappa_{f,s}^e\left(=E_f^eA_f\right)$, where E_f^e and $A_f\left(=\pi r_f^2\right)$ are the Young's modulus (1 MPa) and the cross-sectional area of a single fiber, respectively. The bending modulus of a fiber is given by $\kappa_{f,b}^e\left(=E_fI_f\right)$, where $I_f\left(=\pi r_f^4/4\right)$(25). The stretching elastic energy of the *j*-th segment of the *i*-th fiber is given as a function of the difference between the stressed (L_{ij}^e) and unstressed (L_{ij}^{e0}) lengths, and the bending elastic energy as the one of stressed (θ_{ij}^e) and unstressed (θ_{ij}^{e0}) angles at the *j*-th node between two segments in the *i*-th fiber (Fig. S3). The total elastic energy in the *i*-th ECM fiber in the network can be expressed as following:

$$\mathrm{H}_{f,i}^e = \frac{\kappa_{f,s}^e}{2}\sum_{j=1}^{N_i^e}\frac{\left(L_{ij}^e - L_{ij}^{e0}\right)^2}{L_{ij}^{e0}} + \frac{\kappa_{f,b}^e}{2}\sum_{j=1}^{N_i^e}\frac{\left(\theta_{ij}^e - \theta_{ij}^{e0}\right)^2}{L_{ij}^{e0}}. \tag{S1-27}$$

Here, it should be noted that the elastic energy at the *j*-th node in the *i*-th fiber is summed only for coaxial neighbouring nodes. Similarly, the elastic force at the *j*-th node in the *i*-th fiber, $\boldsymbol{F}_{E,ij}^e$, can be derived by using the virtual work theory:

$$\boldsymbol{F}_{E,ij}^e = -\frac{\partial \mathrm{H}_{f,i}^e}{\partial \boldsymbol{x}_{ij}^e} = -\kappa_{f,s}^e\sum_{k=j}^{j+1}\frac{\left(L_{ik}^e - L_{ik}^{e0}\right)}{L_{ik}^{e0}}\frac{\partial L_{ik}^e}{\partial \boldsymbol{x}_{ij}^e} - \kappa_{f,b}^e\sum_{k=j-1}^{j+1}\frac{(\theta_{ik}^e - \theta_{ik}^{e0})}{L_{ik}^{e0}}\frac{\partial \theta_{ik}^e}{\partial \boldsymbol{x}_{ij}^e} \tag{S1-28}$$

where $\theta_{ik}^{e} = \cos^{-1}\left(\hat{\boldsymbol{t}}_{i,k} \cdot \hat{\boldsymbol{t}}_{i,k+1}\right)$, $\hat{\boldsymbol{t}}_{i,k}$ and $\hat{\boldsymbol{t}}_{i,k+1}$ are tangential unit vectors at the k and k+1-st segments in the i-th fiber, respectively, and $\frac{\partial \theta_{f,ik}^{e}}{\partial \boldsymbol{x}_{ij}^{e}} = \frac{-1}{\sqrt{1-\left(\hat{\boldsymbol{t}}_{i,k} \cdot \hat{\boldsymbol{t}}_{i,k+1}\right)^2}}\left(\frac{\partial \hat{\boldsymbol{t}}_{i,k}}{\partial \boldsymbol{x}_{ij}^{e}} \cdot \hat{\boldsymbol{t}}_{i,k+1} + \hat{\boldsymbol{t}}_{i,k} \cdot \frac{\partial \hat{\boldsymbol{t}}_{i,k+1}}{\partial \boldsymbol{x}_{ij}^{e}}\right)$. To solve the dynamics of ECM fiber network, a dynamic equation at the i-th ECM fiber node can be expressed as

$$C_e \frac{d\boldsymbol{x}_i^e}{dt} = \boldsymbol{F}_{FA,i}^{e} + \boldsymbol{F}_{FC,i}^{e} + \boldsymbol{F}_{E,i}^{e}, \quad i = 1, \cdots, N_e. \tag{S1-29}$$

where C_e is a coefficient of dissipation energy for the ECM fiber. $\boldsymbol{F}_{FA,i}^{e}$ and $\boldsymbol{F}_{FC,i}^{e}$ are a FA force and a FC force at the i-th ECM fiber node, respectively. Note that dynamics of ECM fibers is coupled with intracellular mechanics and filopodia penetration dynamics through two equations of $\boldsymbol{F}_{FA,i}^{e} + \boldsymbol{F}_{FA,i}^{c} = 0$, and $\boldsymbol{F}_{FC,i}^{e} + \boldsymbol{F}_{FC,i}^{f} = 0$, respectively.

4) Simulation of reaction diffusion mass transfer

To consider chemical interactions of the ECM fiber network with a cancer cell, we model the degradation, proteolysis, and haptotaxis of the ECM fiber network. Six reaction-diffusion equations for concentrations of MMP-2 (ϕ_1), TIMP-2 (ϕ_2), MT1-MMP (ϕ_3), a ternary complex of MT1-MMP:TIMP-2:proMMP-2 (ϕ_4) (26), ligands (ϕ_5) (or collagen molecules) and ECM (ϕ_6) are numerically solved using Finite Volume Method (FVM) (27). Constitutive partial differential equations for the six biochemical concentrations are summarised in followings (See Fig. S4):

$$\frac{\partial \phi_1}{\partial t} = \nabla \cdot \left(D_{\phi_1} \nabla \phi_1\right) - k_{\phi_1:\phi_2}^{on} \phi_1 \phi_2 + k_{\phi_3:\phi_4}^{on} \phi_3 \phi_4 - k_{\phi_1}^{decay} \phi_1 \tag{S1-30}$$

$$\frac{\partial \phi_2}{\partial t} = \nabla \cdot \left(D_{\phi_2} \nabla \phi_2\right) - k_{\phi_1:\phi_2}^{on} \phi_1 \phi_2 - k_{\phi_2:\phi_3}^{on} \phi_2 \phi_3 + k_{\phi_4}^{off} \phi_4 + \alpha_{\phi_2}\left(x_{base}^{f}\right) \phi_5 \tag{S1-31}$$

$$\frac{\partial \phi_3}{\partial t} = -k_{\phi_2:\phi_3}^{on} \phi_2 \phi_3 + k_{\phi_4}^{off} \phi_4 - k_{\phi_3}^{decay} \phi_3 + \alpha_{\phi_3}\left(x_{base}^{f}\right) \phi_5 \tag{S1-32}$$

$$\frac{\partial \phi_4}{\partial t} = k_{\phi_2:\phi_3}^{on} \phi_2 \phi_3 + k_{\phi_3:\phi_4}^{on} \phi_3 \phi_4 - k_{\phi_4}^{off} \phi_4 \tag{S1-33}$$

$$\frac{\partial \phi_5}{\partial t} = \nabla \cdot \left(D_{\phi_5} \nabla \phi_5\right) - k_{\phi_5}^{decay} \phi_5 + k_{\phi_6}^{deg} \phi_1 \phi_6 \tag{S1-34}$$

$$\frac{\partial \phi_6}{\partial t} = -k_{\phi_6}^{deg} \phi_1 \phi_6 \tag{S1-35}$$

where $k_{\phi_1}^{decay}$ and $k_{\phi_5}^{decay}$ are decay coefficients of MMP-2 (0.0017 s^{-1}), and ligands (0.0001 s^{-1}), respectively. $k_{\phi_5}^{deg}$ is a degradation coefficient of ECM (1.04×10^6 $M^{-1}s^{-1}$). $k_{\phi_1:\phi_2}^{on}$ is a kinetic association rate constant for binding TIMP-2 with MMP2 (5×10^5 $M^{-1}s^{-1}$) and its term physically represents the reduction of MMP-2 by the endogenous soluble inhibitor TIMP-2. $k_{\phi_3:\phi_4}^{on}$ is a kinetic association rate constant for binding the

ternary complex with MT1-MMP ($1.95\times10^{4}M^{-1}s^{-1}$), which results in the release of activated MMP-2. $k_{\phi_2:\phi_3}^{on}$ is a kinetic association rate constant for binding TIMP-2 with MT1-MMP ($2.74\times10^{6}M^{-1}s^{-1}$), and $k_{\phi_4}^{off}$ is a kinetic dissociation rate constant of the ternary complex for unbinding TIMP2 and MT1-MMP ($2\times10^{-4}s^{-1}$). $\alpha_{\phi_2}\left(x_{base}^{f}\right)$ and $\alpha_{\phi_3}\left(x_{base}^{f}\right)$ represent secretion rates of TIMP2 (1.0×10^{-3}M s^{-1}) and MT1-MMP (1.0×10^{-1}M s^{-1}) at the root of a filopodium, respectively. In particular, x_{base}^{f} indicates the bases of filopodia, and MT1-MMP and TIMP-2 secretions at the membrane near the bases of filopodia are modelled as source terms (28).

Method S2: Mathematical derivation of Cell-Probed Stiffness using Continuum Mechanics

Displacements $u_i\left(x\right)$ at the point $x_i \neq \xi_i$ by the force F_i applied at ξ_i are expressed as

$$u_i\left(x\right) = G_{ij}F_j \tag{S2-1}$$

where G_{ij} is a component of Green's function (30), and it is expressed as

$$G_{ij} = \frac{1+\nu}{8\pi E\left(1-\nu\right)r}\left(\left(3-4\nu\right)\delta_{ij} + \frac{\left(x_i-\xi_i\right)\left(x_j-\xi_j\right)}{r^2}\right). \tag{S2-2}$$

where E is Young's modulus, ν is Poisson's ratio, and $r = \left\|\boldsymbol{x}-\boldsymbol{\xi}\right\|$. For simplicity, Eq. (S2-1) can be expressed as following:

$$u_i = \frac{\alpha}{r}F_i + \frac{\beta}{r}n_i n_j F_j \tag{S2-3}$$

where $\alpha = \frac{\left(1+\nu\right)\left(3-4\nu\right)}{8\pi E\left(1-\nu\right)}$, $\beta = \frac{\left(1+\nu\right)}{8\pi E\left(1-\nu\right)}$, and $n_i = \frac{\left(x_i-\xi_i\right)}{r}$. Inversely, applied force F_i can be expressed by displacements $u_i\left(x\right)$ at the point $x_i \neq \xi_i$ as following:

$$F_i = G_{ij}^{-1}u_j \tag{S2-4}$$

where $G_{ij}^{-1} = \frac{r}{\alpha}\delta_{ij} - \frac{\beta r}{\alpha\left(\alpha+\beta\right)}n_i n_j$. Total time derivative of force, $\frac{dF_i}{dt} = \frac{dF_i\left(\boldsymbol{u}\right)}{dt}$, can be expressed as

$$\frac{dF_i}{dt} = \frac{\partial F_i}{\partial t} + \frac{\partial F_i}{\partial u_j}\frac{\partial u_j}{\partial t}. \tag{S2-5}$$

Since $\frac{\partial F_i}{\partial t}$ =0, and $\frac{\partial F_i}{\partial u_j} = \frac{\partial\left(G_{ij}^{-1}u_j\right)}{\partial u_j} = G_{ij}^{-1}$, the equation (S2-5) becomes

$$\frac{dF_i}{dt} = G_{ij}^{-1}\frac{\partial u_j}{\partial t}. \tag{S2-6}$$

The magnitude of rate of force vector by time $\left\|\frac{d\boldsymbol{F}}{dt}\right\|$ can be calculated as follows:

$$\left\|\frac{d\boldsymbol{F}}{dt}\right\|^2 = \left(\frac{r}{\alpha}\frac{\partial u_i}{\partial t} - \frac{\beta r}{\alpha(\alpha+\beta)} n_i n_j \frac{\partial u_j}{\partial t}\right)\left(\frac{r}{\alpha}\frac{\partial u_i}{\partial t} - \frac{\beta r}{\alpha(\alpha+\beta)} n_i n_k \frac{\partial u_k}{\partial t}\right)$$
$$= \frac{r^2}{\alpha^2}\frac{\partial u_i}{\partial t}\frac{\partial u_i}{\partial t} - \frac{2\beta r^2}{\alpha^2(\alpha+\beta)}\frac{\partial u_i}{\partial t} n_i \frac{\partial u_j}{\partial t} n_j + \frac{\beta^2}{\alpha^2(\alpha+\beta)^2}\frac{\partial u_j}{\partial t} n_j \frac{\partial u_k}{\partial t} n_k \tag{S2-7}$$

$$\left\|\frac{d\boldsymbol{F}}{dt}\right\|^2 = \frac{r^2}{\alpha^2}\left\|\frac{\partial \boldsymbol{u}}{\partial t}\right\|^2 - \frac{r^2(\beta^2+2\alpha\beta)}{\alpha^2(\alpha+\beta)^2}\left(\frac{\partial \boldsymbol{u}}{\partial t}\cdot\boldsymbol{n}\right)^2 \tag{S2-8}$$

Since $\left\|\frac{\partial \boldsymbol{u}}{\partial t}\right\|^2 = \left(\frac{\partial \boldsymbol{u}}{\partial t}\cdot\boldsymbol{n}\right)^2 + \left\|\frac{\partial \boldsymbol{u}}{\partial t}\times\boldsymbol{n}\right\|^2$, Eq. (S2-9) can be expressed as

$$\left\|\frac{d\boldsymbol{F}}{dt}\right\|^2 = \frac{r^2}{(\alpha+\beta)^2}\left(\frac{\partial \boldsymbol{u}}{\partial t}\cdot\boldsymbol{n}\right)^2 + \frac{r^2}{\alpha^2}\left\|\frac{\partial \boldsymbol{u}}{\partial t}\times\boldsymbol{n}\right\|^2 \tag{S2-9}$$

Substituting $\alpha = \frac{(1+\nu)(3-4\nu)}{8\pi E(1-\nu)}$, and $\beta = \frac{(1+\nu)}{8\pi E(1-\nu)}$ into Eq. (S2-9) yields

$$\left\|\frac{d\boldsymbol{F}}{dt}\right\| = \frac{2\pi E r}{(1+\nu)}\sqrt{\left(\frac{\partial \boldsymbol{u}}{\partial t}\cdot\boldsymbol{n}\right)^2 + \frac{16(1-\nu)^2}{(3-4\nu)^2}\left\|\frac{\partial \boldsymbol{u}}{\partial t}\times\boldsymbol{n}\right\|^2} \tag{S2-10}$$

Since $\frac{\partial \boldsymbol{u}}{\partial t} = \boldsymbol{v}$ is velocity vector of displacement with time ($\boldsymbol{v}$) at $x_i \neq \xi_i$, and Eq. (S2-10) can be converted as

$$\left\|\frac{d\boldsymbol{F}}{dt}\right\| = \frac{2\pi E r}{(1+\nu)}\sqrt{(\boldsymbol{v}\cdot\boldsymbol{n})^2 + \frac{16(1-\nu)^2}{(3-4\nu)^2}\|\boldsymbol{v}\times\boldsymbol{n}\|^2}. \tag{S2-11}$$

Thus, the equation for calculating the effective local stiffness, E^*, at the point $x_i \neq \xi_i$ can be expressed as

$$E^* = \frac{(1+\nu)\left\|\frac{d\boldsymbol{F}}{dt}\right\|}{2\pi r v_t} \tag{S2-12}$$

where v_t is a total speed of displacement implies a vector summation of two orthogonal components of an axial speed $(\boldsymbol{v}\cdot\boldsymbol{n})$ and a transverse speed $\left(\frac{4(1-\nu)}{(3-4\nu)}\|\boldsymbol{v}\times\boldsymbol{n}\|\right)$, and it is expressed as

$$v_t = \sqrt{(\boldsymbol{v}\cdot\boldsymbol{n})^2 + \frac{16(1-\nu)^2}{(3-4\nu)^2}\|\boldsymbol{v}\times\boldsymbol{n}\|^2}. \tag{S2-13}$$

To compute effective Cell-Probed Stiffness (CPS), $\bar{E}^*$, at the *i*-th filopodium which has a finite number of focal complexes (FCs) and interacts with a number of ECM fiber nodes, an error, ϕ_{km}, between the *k*-th FC and the *m*-th ECM fiber node as the square of the difference $\left\|\frac{d\boldsymbol{F}}{dt}\right\|_k$ at the *k*-th FC and $\frac{2\pi E^* r_{km} v_{t,km}}{(1+\nu)}$ is defined by

$$\phi_{km} = \left(\left\| \frac{d\boldsymbol{F}}{dt} \right\|_k - \frac{2\pi E^* r_{km} v_{t,km}}{(1+\nu)} \right)^2 . \tag{S2-14}$$

where $r_{k,m} = \left\| \boldsymbol{x}_m - \boldsymbol{\xi}_k \right\|$, $v_{t,km} = \sqrt{(\boldsymbol{v}_m \cdot \boldsymbol{n}_{km})^2 + \frac{16(1-\nu)^2}{(3-4\nu)^2} \left\| \boldsymbol{v}_m \times \boldsymbol{n}_{km} \right\|^2}$, $\boldsymbol{v}_m$ is a velocity vector at the m-th fiber node, and $\boldsymbol{n}_{km}$ is a unit vector in the direction of $(\boldsymbol{x}_m - \boldsymbol{\xi}_k)$.

From the simulation of filopodia-ECM fiber interactions, a time series of force $\boldsymbol{F}$ and displacement $\boldsymbol{u}$ are available. The local stiffness E^* can be selected to best approximate these data. Considering the least square error among all of neighboring nodes of ECM fibers (total number of ECM fiber nodes is *M*) which are interacted by the *k*-th filopodium, and summed least square error at the *k*-th filopodium is expressed as

$$\phi_k = \sum_{m=1}^{M} \phi_{km} = \sum_{m=1}^{M} \left(\left\| \frac{d\boldsymbol{F}}{dt} \right\|_k - \frac{2\pi E^* r_{km} v_{t,km}}{(1+\nu)} \right)^2 . \tag{S2-15}$$

When a total number of FC is *K* on the *i*-th filopodial tip, summed least square error, ϕ_i, at the *i*-th filopodium is expressed as

$$\phi_i = \sum_{k=1}^{K} \phi_k = \sum_{k=1}^{K} \sum_{m=1}^{M} \phi_{km} = \sum_{k=1}^{K} \sum_{m=1}^{M} \left(\left\| \frac{d\boldsymbol{F}}{dt} \right\|_k - \frac{2\pi E^* r_{km} v_{t,km}}{(1+\nu)} \right)^2 \tag{S2-16}$$

The effective CPS, $\bar{E}^*$,is solved by minimizing ϕ_i with respect to E^*. Thus, $\frac{\partial \phi_i}{\partial E^*} = 0$ is expressed as

$$\frac{\partial \phi_i}{\partial E^*} = \sum_{k=1}^{K} \sum_{m=1}^{M} \left(\left\| \frac{d\boldsymbol{F}}{dt} \right\|_k - \frac{2\pi E^* r_{km} v_{t,km}}{(1+\nu)} \right) r_{km} v_{t,km} = 0. \tag{S2-17}$$

Thus, $\bar{E}^*$ is expressed as

$$\bar{E}^* = \frac{(1+\nu)}{2\pi} \frac{\sum_{k=1}^{K} \left[\left\| \frac{d\boldsymbol{F}}{dt} \right\|_k \sum_{m=1}^{M} \left(r_{km} v_{t,km} \right) \right]}{\sum_{k=1}^{K} \sum_{m=1}^{M} \left(r_{km} v_{t,km} \right)^2}. \tag{S2-18}$$

Method S3: Mathematical derivation of Cell-Probed Stiffness using discrete ECM fiber Mechanics

Approach 1)

Elastic energy of an ECM fiber can be expressed as

$$E_f = \frac{1}{2} k_f \left(L_1^f - L_0^f \right)^2 \tag{S3-1}$$

where k_f is line stiffness of ECM fiber, L_0 and L_1 are lengths of unstressed and stressed ECM fiber, respectively. $L_1^f = \left\| \boldsymbol{x}_1^f - \boldsymbol{x}_2^f \right\|$. Using the virtual energy method, elastic force, F_i, acting on $\boldsymbol{x}_1^f$ can be expressed as

$$F_i = -\frac{\partial E_f}{\partial x_{1i}^f} = -k_f\left(L_1^f - L_0^f\right)\frac{\left(x_{1i}^f - x_{2i}^f\right)}{L_1^f}. \tag{S3-2}$$

The rate of elastic force by time can be expressed as

$$\frac{dF_i}{dt} = -k_f\left(\left(\frac{dL_1^f}{dt}\right)\frac{\left(x_{1i}^f - x_{2i}^f\right)}{L_1^f} - \left(L_1^f - L_0^f\right)\frac{\left(x_{1i}^f - x_{2i}^f\right)}{L_1^{f2}}\left(\frac{dL_1^f}{dt}\right) + \left(L_1^f - L_0^f\right)\frac{\left(v_{1i}^f - v_{2i}^f\right)}{L_1^f}\right) \tag{S3-3}$$

where v_{1i}^f and v_{2i}^f are *i*-th components of velocities of nodes, $\boldsymbol{x}_1^f$ and $\boldsymbol{x}_2^f$, respectively. Then, $\left\|\frac{dF}{dt}\right\|^2$ is can be calculated as followings:

$$\left\|\frac{dF}{dt}\right\|^2 = \frac{k_f^2}{L_1^{f2}}\left\|\left(\frac{dL_1^f}{dt}\right)\left(x_{1i}^f - x_{2i}^f\right) - \left(L_1^f - L_0^f\right)\frac{\left(x_{1i}^f - x_{2i}^f\right)}{L_1^f}\left(\frac{dL_1^f}{dt}\right) + \left(L_1^f - L_0^f\right)\left(v_{1i}^f - v_{2i}^f\right)\right\|^2 \tag{S3-4}$$

Equation (S3-4) can be simplified as

$$\left\|\frac{dF}{dt}\right\|^2 = \frac{k_f^2}{L_1^{f2}}\left(\begin{array}{l}\left(\frac{dL_1^f}{dt}\right)^2\left\|\boldsymbol{x}_1^f - \boldsymbol{x}_2^f\right\|^2\left(\frac{\left(L_1^f - L_0^f\right)}{L_1^f} - 1\right)^2 + 2\frac{\partial L_1}{\partial t}\left(L_1^f - L_0^f\right)\left(1 - \frac{\left(L_1^f - L_0^f\right)}{L_1^f}\right)\left(\boldsymbol{v}_1^f - \boldsymbol{v}_2^f\right)\cdot\left(\boldsymbol{x}_1^f - \boldsymbol{x}_2^f\right) \\ + \frac{\left(L_1^f - L_0^f\right)^2}{L_1^{f2}}\left(\left(\left(\boldsymbol{v}_1^f - \boldsymbol{v}_2^f\right)\cdot\left(\boldsymbol{x}_1^f - \boldsymbol{x}_2^f\right)\right)^2 + \left\|\left(\boldsymbol{v}_1^f - \boldsymbol{v}_2^f\right)\times\left(\boldsymbol{x}_1^f - \boldsymbol{x}_2^f\right)\right\|^2\right)\end{array}\right). \tag{S3-5}$$

Since $\boldsymbol{n}^f = \frac{\left(\boldsymbol{x}_1^f - \boldsymbol{x}_2^f\right)}{L_1^f}$, equation (S3-5) can be further simplified as

$$\left\|\frac{dF}{dt}\right\|^2 = \frac{k_f^2}{L_1^{f2}}\left(\begin{array}{l}\left(\frac{dL_1^f}{dt}\right)^2 L_0^{f2} + 2\frac{\partial L_1^f}{\partial t}\left(L_1^f - L_0^f\right)L_0^f\left(\boldsymbol{v}_1^f - \boldsymbol{v}_2^f\right)\cdot\boldsymbol{n}^f \\ + \left(L_1^f - L_0^f\right)^2\left(\left(\left(\boldsymbol{v}_1^f - \boldsymbol{v}_2^f\right)\cdot\boldsymbol{n}^f\right)^2 + \left\|\left(\boldsymbol{v}_1^f - \boldsymbol{v}_2^f\right)\times\boldsymbol{n}^f\right\|^2\right)\end{array}\right) \tag{S3-6}$$

or,

$$\left\|\frac{dF}{dt}\right\|^2 = \frac{k_f^2}{L_1^{f2}}\left(\left(\frac{dL_1^f}{dt}L_0^f + \left(L_1^f - L_0^f\right)\left(\left(\boldsymbol{v}_1^f - \boldsymbol{v}_2^f\right)\cdot\boldsymbol{n}^f\right)\right)^2 L_0^{f2} + \left(L_1^f - L_0^f\right)^2\left\|\left(\boldsymbol{v}_1^f - \boldsymbol{v}_2^f\right)\times\boldsymbol{n}^f\right\|^2\right). \tag{S3-7}$$

Since $\frac{dL_1^f}{dt} = \frac{dL_1^f\left(\boldsymbol{x}_1^f, \boldsymbol{x}_2^f\right)}{dt} = \left(\boldsymbol{v}_1^f - \boldsymbol{v}_2^f\right)\cdot\boldsymbol{n}^f$, equation (S3-7) can be further simplified as

$$\left\|\frac{dF}{dt}\right\|^2 = k_f^2\left(\left(\left(\boldsymbol{v}_1^f - \boldsymbol{v}_2^f\right)\cdot\boldsymbol{n}^f\right)^2 + \left(\frac{L_1^f - L_0^f}{L_1^f}\right)^2\left\|\left(\boldsymbol{v}_1^f - \boldsymbol{v}_2^f\right)\times\boldsymbol{n}^f\right\|^2\right). \tag{S3-8}$$

Thus, the equation for calculating the effective stiffness of fiber, k_f^*, can be expressed as

$$k_f^* = \left\|\frac{dF}{dt}\right\| \Big/ v_t^f \tag{S3-9}$$

$$v_t^f = \sqrt{\left(\left(\boldsymbol{v}_1^f - \boldsymbol{v}_2^f\right)\cdot \boldsymbol{n}^f\right)^2 + \left(\frac{L_1^f - L_0^f}{L_1^f}\right)^2 \left\|\left(\boldsymbol{v}_1^f - \boldsymbol{v}_2^f\right)\times \boldsymbol{n}^f\right\|^2} \tag{S3-10}$$

where $\left\|\frac{d\boldsymbol{F}}{dt}\right\|$ represents the rate of traction force by time at the filopodial tip with an assumption that the rate of traction force by time and the rate of elastic force of ECM fiber by time are equal, and v_t^f is the total speed of displacement of the fiber.

Approach 2)

Total time derivative of force at the first node of fiber, $\frac{dF_{1i}}{dt} = \frac{dF_{1i}\left(\boldsymbol{x}_1^f, \boldsymbol{x}_2^f\right)}{dt}$, can be expressed as

$$\frac{dF_{1i}}{dt} = \frac{\partial F_{1i}}{\partial t} + \frac{\partial F_{1i}}{\partial x_{1j}^f}\frac{\partial x_{1j}^f}{\partial t} + \frac{\partial F_{1i}}{\partial x_{2j}^f}\frac{\partial x_{2j}^f}{\partial t}. \tag{S3-11}$$

Since $\frac{\partial F_{1i}}{\partial t}$=0, $\frac{\partial F_{1i}}{\partial x_{2j}^f} = -\frac{\partial F_{1i}}{\partial x_{1j}^f}$, and $F_{1i} = -\frac{\partial E_f}{\partial x_{1i}^f}$, the equation (S3-11) becomes

$$\frac{dF_{1i}}{dt} = -\frac{\partial^2 E_f}{\partial x_{1i}^f \partial x_{1j}^f}\left(\frac{\partial x_{1j}^f}{\partial t} - \frac{\partial x_{2j}^f}{\partial t}\right). \tag{S3-12}$$

Let $K_{ij} = \frac{\partial^2 E_f}{\partial x_{1i}^f \partial x_{1j}^f}$ be is a component of the stiffness matrix K, $v_{1j}^f - v_{2j}^f = \frac{\partial x_{1j}^f}{\partial t} - \frac{\partial x_{2j}^f}{\partial t}$ be the difference of velocity between two nodes on the fiber, and $\frac{dF_i}{dt} = -\frac{dF_{1i}}{dt}$ be the rate of force by time at the filopodial tip, the equation (S3-12) becomes

$$\frac{dF_i}{dt} = K_{ij}\left(v_{1j}^f - v_{2j}^f\right) \tag{S3-13}$$

$$K_{ij} = k_f\left(\left(1 - \frac{L_0^f}{L_1^f}\right)\delta_{ij} + \frac{L_0^f}{L_1^f}\frac{\left(x_{1i}^f - x_{2i}^f\right)}{L_1^f}\frac{\left(x_{1j}^f - x_{2j}^f\right)}{L_1^f}\right). \tag{S3-14}$$

For simplicity, Eq. (S3-14) can be expressed using the indicial notation as following:

$$\frac{dF_i}{dt} = k_f\left(1-S\right)\left(v_{1i}^f - v_{2i}^f\right) + k_f S\, n_{f,i} n_{f,j}\left(v_{1j}^f - v_{2j}^f\right) \tag{S3-15}$$

where $S = \frac{L_0^f}{L_1^f}$, and $n_i^f = \frac{\left(x_{1i}^f - x_{2i}^f\right)}{L_1^f}$. The magnitude of $\frac{d\boldsymbol{F}}{dt}$ can be calculated as follows:

$$\begin{aligned}
\left\|\frac{d\boldsymbol{F}}{dt}\right\|^2 &= \left(-\frac{dF_i}{dt}\right)\left(-\frac{dF_i}{dt}\right) \\
&= k_f^2\left(\left(1-S\right)\left(v_{1i}^f - v_{2i}^f\right) + S\, n_{f,i} n_{f,j}\left(v_{1j}^f - v_{2j}^f\right)\right)\left(\left(1-S\right)\left(v_{1i}^f - v_{2i}^f\right) + S\, n_{f,i} n_{f,k}\left(v_{1k}^f - v_{2k}^f\right)\right) \\
&= k_f^2\left(\left(1-S\right)^2\left\|\boldsymbol{v}_1^f - \boldsymbol{v}_2^f\right\|^2 + 2\left(1-S\right)S\left(\left(\boldsymbol{v}_1^f - \boldsymbol{v}_2^f\right)\cdot \boldsymbol{n}^f\right)^2 + S^2\left(\left(\boldsymbol{v}_1^f - \boldsymbol{v}_2^f\right)\cdot \boldsymbol{n}^f\right)^2\right)
\end{aligned} \tag{S3-16}$$

$$\left\|\frac{d\boldsymbol{F}}{dt}\right\|^2 = k_f^2\left(\left(1-S\right)^2\left\|\boldsymbol{v}_1^f-\boldsymbol{v}_2^f\right\|^2+\left(2S-S^2\right)\left(\left(\boldsymbol{v}_1^f-\boldsymbol{v}_2^f\right)\cdot\boldsymbol{n}^f\right)^2\right) \tag{S3-17}$$

Since $\left\|\boldsymbol{v}_1^f-\boldsymbol{v}_2^f\right\|^2=\left(\left(\boldsymbol{v}_1^f-\boldsymbol{v}_2^f\right)\cdot\boldsymbol{n}^f\right)^2+\left\|\left(\boldsymbol{v}_1^f-\boldsymbol{v}_2^f\right)\times\boldsymbol{n}^f\right\|^2$, Eq. (S3-17) can be expressed as

$$\left\|\frac{d\boldsymbol{F}}{dt}\right\| = k_f\sqrt{\left(\left(\boldsymbol{v}_1^f-\boldsymbol{v}_2^f\right)\cdot\boldsymbol{n}^f\right)^2+\left(1-S\right)^2\left\|\left(\boldsymbol{v}_1^f-\boldsymbol{v}_2^f\right)\times\boldsymbol{n}^f\right\|^2}. \tag{S3-18}$$

Therefore, the equation for calculating the effective stiffness of fiber, k_f^*, is identical as Equation (S3-9). Similarly, to compute effective Cell-Probed Stiffness of fiber (CPSF), $\bar{k}_f^*$, at the *i*-th filopodium which has a finite number of focal complexes (FCs) and interacts with a number of segmented ECM fibers (*M*). Since the fiber is serially connected, effective stiffness of the fiber can be expressed as

$$k_f^* = \left\|\frac{dF}{dt}\right\| \Big/ \sum_{m=1}^{M} v_{t,m}^f \tag{S3-19}$$

where $v_{t,m}^f = \sqrt{\left(\left(\boldsymbol{v}_{m1}^f-\boldsymbol{v}_{m2}^f\right)\cdot\boldsymbol{n}_m^f\right)^2+\left(1-\frac{L_{m0}^f}{L_{m1}^f}\right)^2\left\|\left(\boldsymbol{v}_{m1}^f-\boldsymbol{v}_{m2}^f\right)\times\boldsymbol{n}_m^f\right\|^2}$, $\boldsymbol{v}_{m1}^f$ and $\boldsymbol{v}_{m2}^f$ are velocity vectors of two end nodes at the *m*-th fiber, respectively, and $\boldsymbol{n}_m^f$ is a unit vector in the direction of $\left(\boldsymbol{x}_{m1}^f-\boldsymbol{x}_{m2}^f\right)$.

Then, error, ϕ_k, between the *k*-th FC and serially connected ECM fibers (number of nodes on these fiber is *M*+1) as the square of the difference $\left\|\frac{d\boldsymbol{F}}{dt}\right\|_k$ at the *k*-th FC and $k_f^*\sum_{m=1}^{M} v_{t,m}^f$ is defined by

$$\phi_k = \left(\left\|\frac{d\boldsymbol{F}}{dt}\right\|_k - k_f^*\sum_{m=1}^{M} v_{t,m}^f\right)^2. \tag{S3-20}$$

From the simulation of filopodia-ECM fiber interactions, a time series of force $\boldsymbol{F}$ and displacement $\boldsymbol{u}$ are available. The local stiffness k_f^* can be selected to best approximate these data. Considering the least square error among all of neighboring of segmented ECM fibers (total number of segmented ECM fiber is *M*) which are interacted by the *k*-th filopodium, and summed least square error at the *k*-th node on the filopodium.

When a total number of FC is *K* on the *i*-th filopodial tip, summed least square error, ϕ_i, at the *i*-th filopodium is expressed as

$$\phi_i = \sum_{k=1}^{K}\phi_k = \sum_{k=1}^{K}\sum_{m=1}^{M}\phi_{km} = \sum_{k=1}^{K}\left(\left\|\frac{d\boldsymbol{F}}{dt}\right\|_k - k_f^*\sum_{m=1}^{M} v_{t,m}^f\right)^2 \tag{S3-21}$$

The effective CPS, $\bar{k}_f^*$, is solved by minimizing ϕ_i with respect to k_f^*. Thus, $\frac{\partial\phi_i}{\partial k_f^*}=0$ is expressed as

$$\frac{\partial \phi_i}{\partial k_f^*} = \sum_{k=1}^{K}\left(\left(\left\|\frac{d\boldsymbol{F}}{dt}\right\|_k - k_f^*\sum_{m=1}^{M} v_{t,m}^f\right)\left(\sum_{m=1}^{M} v_{t,m}^f\right)\right) = 0. \tag{S3-22}$$

Thus, $\bar{k}_f^*$ is expressed as

$$\bar{k}_f^* = \frac{\sum_{k=1}^{K}\left[\left\|\frac{d\boldsymbol{F}}{dt}\right\|_k \sum_{m=1}^{M} v_{t,m}^f\right]}{\sum_{k=1}^{K}\left[\left(\sum_{m=1}^{M} v_{t,m}^f\right)^2\right]}. \tag{S3-23}$$

Method S4: Computation of stress and strain in 3D ECM

1) Computation of strain fields

The strain tensor ε is symmetry and its components can be expressed with respect to x_1, x_2, and x_3 coordinate systems as following:

$$[\varepsilon] = \begin{pmatrix} \varepsilon_{11} & \varepsilon_{12} & \varepsilon_{13} \\ \varepsilon_{12} & \varepsilon_{22} & \varepsilon_{23} \\ \varepsilon_{13} & \varepsilon_{23} & \varepsilon_{33} \end{pmatrix} \tag{S4-1}$$

Strain components:

$$\varepsilon_{ij} = \frac{1}{2}\left(\frac{\partial u_i}{\partial x_j} + \frac{\partial u_j}{\partial x_i}\right) \tag{S4-2}$$

In order to calculate $\frac{\partial u_i}{\partial x_i}$ and $\frac{\partial u_i}{\partial x_j}$ using indicial notation, the Equation (S2-1) can be expressed as following:

$$u_i = \frac{\gamma(3-4\nu)}{r}F_i + \frac{\gamma(x_i-\zeta_i)(x_j-\zeta_j)}{r^3}F_j \tag{S4-3}$$

where $\gamma = \frac{(1+\nu)}{8\pi E(1-\nu)}$. Then, if we differentiate u_i with respect to x_i and write $\frac{\partial u_i}{\partial x_i} = \partial\left(\frac{\gamma(3-4\nu)}{r}F_i + \frac{\gamma(x_i-\zeta_i)(x_j-\zeta_j)}{r^3}F_j\right)\Big/\partial x_i$, we would violate rules of indicial notation that the right-hand side of the equation has the subscript *i* appearing three times in one symbol grouping (29). In order to solve this difficulty, we make use of the fact the specific choice of the index in a dummy subscript is not significant and so we can rewrite $u_i = \frac{\gamma(3-4\nu)}{r}F_p + \frac{\gamma(x_p-\zeta_p)(x_q-\zeta_q)}{r^3}F_q$. Then $\frac{\partial u_i}{\partial x_i}$ can be calculated as followings:

$$\frac{\partial u_i}{\partial x_i} = \partial\left(\frac{\gamma(3-4\nu)}{r}F_p + \frac{\gamma(x_p-\zeta_p)(x_q-\zeta_q)}{r^3}F_q\right)\Big/\partial x_i$$
$$= -\frac{\gamma(3-4\nu)}{r^2}\frac{\partial r}{\partial x_i}F_p + \frac{\gamma\frac{\partial x_p}{\partial x_i}(x_q-\zeta_q)}{r^3}F_q + \frac{\gamma(x_p-\zeta_p)\frac{\partial x_q}{\partial x_i}}{r^3}F_q - \frac{3\gamma(x_p-\zeta_p)(x_q-\zeta_q)\frac{\partial r}{\partial x_i}}{r^4}F_q \quad \text{(S4-4)}$$

Here, $\frac{\partial r}{\partial x_i} = \frac{(x_p-\zeta_p)}{r}\frac{\partial x_p}{\partial x_i}$, and substituting $\frac{\partial r}{\partial x_i}$ into Equation (S4-4) yields

$$\frac{\partial u_i}{\partial x_i} = -\frac{\gamma(3-4\nu)(x_p-\zeta_p)}{r^3}\frac{\partial x_p}{\partial x_i}F_p + \frac{\gamma\frac{\partial x_p}{\partial x_i}(x_q-\zeta_q)}{r^3}F_q + \frac{\gamma(x_p-\zeta_p)\frac{\partial x_q}{\partial x_i}}{r^3}F_q - \frac{3\gamma(x_p-\zeta_p)^2(x_q-\zeta_q)\frac{\partial x_p}{\partial x_i}}{r^5}F_q \quad \text{(S4-5)}$$

Since x_p and x_q are independent variables, it follows that $\frac{\partial x_p}{\partial x_i} = \delta_{pi}$ and $\frac{\partial x_q}{\partial x_i} = \delta_{qi}$.

Using this above gives

$$\frac{\partial u_i}{\partial x_i} = -\frac{\gamma(3-4\nu)(x_p-\zeta_p)}{r^3}\delta_{pi}F_p + \frac{\gamma\delta_{pi}(x_q-\zeta_q)}{r^3}F_q + \frac{\gamma(x_p-\zeta_p)\delta_{qi}}{r^3}F_q - \frac{3\gamma(x_p-\zeta_p)^2(x_q-\zeta_q)\delta_{pi}}{r^5}F_q \quad \text{(S4-6)}$$

By the substation rule, the above equation simplifies to

$$\frac{\partial u_i}{\partial x_i} = -\frac{\gamma(3-4\nu)(x_i-\zeta_i)}{r^3}F_i + \frac{\gamma(x_j-\zeta_j)}{r^3}F_j + \frac{\gamma(x_i-\zeta_i)}{r^3}F_i - \frac{3\gamma(x_i-\zeta_i)^2(x_j-\zeta_j)}{r^5}F_j. \quad \text{(S4-7)}$$

Further simplifies to

$$\frac{\partial u_i}{\partial x_i} = \frac{\gamma(4\nu-2)(x_i-\zeta_i)}{r^3}F_i + \frac{\gamma(x_j-\zeta_j)}{r^3}\left(1-\frac{3(x_i-\zeta_i)^2}{r^2}\right)F_j. \quad \text{(S4-8)}$$

Similarly, we differentiate u_i with respect to x_j, $\frac{\partial u_i}{\partial x_j}$ can be calculated as followings:

$$\frac{\partial u_i}{\partial x_j} = -\frac{\gamma(3-4\nu)}{r^2}\frac{\partial r}{\partial x_j}F_p + \frac{\gamma\frac{\partial x_p}{\partial x_j}(x_q-\zeta_q)}{r^3}F_q + \frac{\gamma(x_p-\zeta_p)\frac{\partial x_q}{\partial x_j}}{r^3}F_q - \frac{3\gamma(x_p-\zeta_p)(x_q-\zeta_q)\frac{\partial r}{\partial x_j}}{r^4}F_q \quad \text{(S4-9)}$$

Here $\frac{\partial r}{\partial x_j}=\frac{\left(x_k-\zeta_k\right)}{r}\frac{\partial x_k}{\partial x_j}$ where $k\neq i$, and substituting $\frac{\partial r}{\partial x_j}$ and $\frac{\partial x_p}{\partial x_j}$ =0 into Equation (S2-9) yields

$$\frac{\partial u_i}{\partial x_j}=-\frac{\gamma(3-4\nu)\left(x_k-\zeta_k\right)}{r^3}\frac{\partial x_k}{\partial x_j}F_p+\frac{\gamma\left(x_p-\zeta_p\right)\frac{\partial x_q}{\partial x_j}}{r^3}F_q-\frac{3\gamma\left(x_p-\zeta_p\right)\left(x_q-\zeta_q\right)\left(x_k-\zeta_k\right)\frac{\partial x_k}{\partial x_j}}{r^5}F_q \quad \text{(S4-10)}$$

By the substitution rule, the above equation simplifies to

$$\frac{\partial u_i}{\partial x_j}=-\frac{\gamma(3-4\nu)\left(x_j-\zeta_j\right)}{r^3}F_p+\frac{\gamma\left(x_p-\zeta_p\right)}{r^3}F_j-\frac{3\gamma\left(x_p-\zeta_p\right)\left(x_q-\zeta_q\right)\left(x_j-\zeta_j\right)}{r^5}F_q \quad \text{(S4-11)}$$

Or, by substituting *p* and *q* with *i* and *k* yields

$$\frac{\partial u_i}{\partial x_j}=-\frac{\gamma(3-4\nu)\left(x_j-\zeta_j\right)}{r^3}F_i+\frac{\gamma\left(x_i-\zeta_i\right)}{r^3}F_j-\frac{3\gamma\left(x_i-\zeta_i\right)\left(x_j-\zeta_j\right)\left(x_k-\zeta_k\right)}{r^5}F_k \quad \text{(S4-12)}$$

where k is a dummy subscript. Lastly, ε_{ii} and ε_{ij} can be expressed using Equations (S4-8) and (S4-12) as followings:

$$\varepsilon_{ii}=\frac{\partial u_i}{\partial x_i}=\frac{2\gamma(2\nu-1)\left(x_i-\zeta_i\right)}{r^3}F_i+\frac{\gamma\left(x_j-\zeta_j\right)}{r^3}\left(1-\frac{3\left(x_i-\zeta_i\right)^2}{r^2}\right)F_j. \quad \text{(S4-13)}$$

$$\begin{aligned}\varepsilon_{ij}&=\frac{1}{2}\left(\frac{\partial u_i}{\partial x_j}+\frac{\partial u_j}{\partial x_i}\right)\\&=\frac{\gamma(2\nu-1)\left(x_j-\zeta_j\right)}{r^3}F_i+\frac{\gamma(2\nu-1)\left(x_i-\zeta_i\right)}{r^3}F_j-\frac{3\gamma\left(x_i-\zeta_i\right)\left(x_j-\zeta_j\right)\left(x_k-\zeta_k\right)}{r^5}F_k\end{aligned} \quad \text{(S4-14)}$$

Substituting $\gamma=\frac{(1+\nu)}{8\pi E(1-\nu)}$ into above equations gives

$$\varepsilon_{ii}=\frac{(1+\nu)(2\nu-1)\left(x_i-\zeta_i\right)}{8\pi E(1-\nu)r^3}F_i+\frac{(1+\nu)\left(x_j-\zeta_j\right)}{8\pi E(1-\nu)r^3}\left(1-\frac{3\left(x_i-\zeta_i\right)^2}{r^2}\right)F_j. \quad \text{(S4-15)}$$

$$\begin{aligned}\varepsilon_{ij}=&\frac{(1+\nu)(2\nu-1)\left(x_j-\zeta_j\right)}{8\pi E(1-\nu)r^3}F_i+\frac{(1+\nu)(2\nu-1)\left(x_i-\zeta_i\right)}{8\pi E(1-\nu)r^3}F_j\\&-\frac{3(1+\nu)\left(x_i-\zeta_i\right)\left(x_j-\zeta_j\right)\left(x_k-\zeta_k\right)}{8\pi E(1-\nu)r^5}F_k\end{aligned} \quad \text{(S4-16)}$$

2) Computation of stress fields

Stress tensor is symmetry, and its components can be expressed with respect to x_1, x_2, and x_3 coordinate systems as following:

$$[\sigma]=\begin{pmatrix}\sigma_{11} & \sigma_{12} & \sigma_{13}\\ \sigma_{12} & \sigma_{22} & \sigma_{23}\\ \sigma_{13} & \sigma_{23} & \sigma_{33}\end{pmatrix} \tag{S4-17}$$

In indicial notation, stress fields can be expressed using strain-stress relation for isotropic materials:

$$\sigma_{ij}=\lambda u_{k,k}\delta_{ij}+\mu\left(u_{i,j}+u_{j,i}\right), \tag{S4-18}$$

Diagonal components σ_{ii} can be expressed as followings:

$$\sigma_{ii}=\frac{E}{1+\nu}\varepsilon_{ii}+\frac{E\nu}{(1+\nu)(1-2\nu)}\varepsilon_{kk} \tag{S4-19}$$

Substituting Equation (S4-15) into the above equation gives

$$\begin{aligned}\sigma_{ii}=&\frac{(4\nu-2)(x_i-\zeta_i)}{8\pi(1-\nu)r^3}F_i+\frac{(x_j-\zeta_j)}{8\pi(1-\nu)r^3}\left(1-\frac{3(x_i-\zeta_i)^2}{r^2}\right)F_j+\\ &\frac{-2\nu(x_k-\zeta_k)}{8\pi(1-\nu)r^3}F_k+\frac{\nu}{(1-2\nu)}\frac{(x_j-\zeta_j)}{8\pi(1-\nu)r^3}\left(\delta_{kk}-\frac{3(x_k-\zeta_k)^2}{r^2}\right)F_j.\end{aligned} \tag{S4-20}$$

Here the last term in the LHS vanishes because $\delta_{kk}-\frac{3(x_k-\zeta_k)^2}{r^2}=3-\frac{3r^2}{r^2}=0$, and changing subscript k to j gives

$$\sigma_{ii}=\frac{(4\nu-2)(x_i-\zeta_i)}{8\pi(1-\nu)r^3}F_i+\frac{(x_j-\zeta_j)}{8\pi(1-\nu)r^3}\left(1-2\nu-\frac{3(x_i-\zeta_i)^2}{r^2}\right)F_j. \tag{S4-21}$$

Similarly, σ_{ij}, where $i\neq j$ can be expressed as

$$\sigma_{ij}=\frac{E}{(1+\nu)}\varepsilon_{ij} \tag{S4-22}$$

Substituting Equation (S4-16) into the above equation gives

$$\sigma_{ij}=\frac{(2\nu-1)(x_j-\zeta_j)}{8\pi(1-\nu)r^3}F_i+\frac{(2\nu-1)(x_i-\zeta_i)}{8\pi(1-\nu)r^3}F_j-\frac{3(x_i-\zeta_i)(x_j-\zeta_j)(x_k-\zeta_k)}{8\pi(1-\nu)r^5}F_k. \tag{S4-23}$$

It should be noted that Eq. (S4-21) and (S4-23) are expressed without the modulus E.

As shown in Fig. S15, when a node of $\boldsymbol{x}$ is connected with neighboring nodes of $\boldsymbol{\zeta}^1, \boldsymbol{\zeta}^2, \boldsymbol{\zeta}^3$, and $\boldsymbol{\zeta}^4$ where forces of $\boldsymbol{F}^1, \boldsymbol{F}^2, \boldsymbol{F}^3$, and $\boldsymbol{F}^4$ are respectively exerted, components of average stress tensor at the node of $\boldsymbol{x}$ can be expressed as followings:

$$\bar{\sigma}_{ii} = \frac{1}{N}\sum_{m=1}^{N}\sigma_{ii}^{m} = \frac{1}{N}\sum_{m=1}^{N}\frac{(4\nu-2)\left(x_i-\zeta_i^m\right)}{8\pi(1-\nu)r_m^3}F_i^m + \frac{\left(x_j-\zeta_j^m\right)}{8\pi(1-\nu)r_m^3}\left(1-2\nu-\frac{3\left(x_i-\zeta_i^m\right)^2}{r_m^2}\right)F_j^m, \tag{S4-24}$$

$$\begin{aligned}\bar{\sigma}_{ij} &= \frac{1}{N}\sum_{m=1}^{N}\sigma_{ij}^{m} \\ &= \frac{1}{N}\sum_{m=1}^{N}\frac{(2\nu-1)\left(x_j-\zeta_j^m\right)}{8\pi(1-\nu)r_m^3}F_i^m + \frac{(2\nu-1)\left(x_i-\zeta_i^m\right)}{8\pi(1-\nu)r_m^3}F_j^m - \frac{3\left(x_i-\zeta_i^m\right)\left(x_j-\zeta_j^m\right)\left(x_k-\zeta_k^m\right)}{8\pi(1-\nu)r_m^3}F_k^m\end{aligned} \tag{S4-25}$$

where N is the number of neighboring nodes which connect with the node of x. Superscripts or subscript m of ζ_i^m, F_i^m, and r_m indicate the m-th neighboring node.

3) Discrete deformation gradient method

In continuum mechanics, the finite deformation of a body maps initial location vector, $\boldsymbol{X}$, in the reference configuration Ω_0 to current location vector, $\boldsymbol{x}$, in the current configuration Ω_1, and its mapping M (Fig. S16) is indicated by

$$\boldsymbol{x} = \mathrm{M}(\boldsymbol{X}). \tag{S4-21}$$

The derivative of this deformation is known as the deformation gradient $\boldsymbol{F}$, and it is defined as

$$\boldsymbol{F} \equiv \frac{\partial \mathrm{M}(\boldsymbol{X})}{\partial \boldsymbol{X}} = \frac{\partial \boldsymbol{x}}{\partial \boldsymbol{X}}. \tag{S4-22}$$

The Lagrangian or Green strain tensor, $\boldsymbol{E}$, is given by

$$\boldsymbol{E} = \frac{1}{2}\left(\boldsymbol{F}^T\boldsymbol{F} - \boldsymbol{I}\right). \tag{S4-23}$$

Next, we consider the discrete deformation gradient which has been applied to the area of atomistic simulations of materials (30). We applied similar approach of the discrete deformation gradient to the discrete ECM fiber mechanics. As shown in Fig. S16, vectors $\Delta\boldsymbol{X}_{ij}$ and $\Delta\boldsymbol{x}_{ij}$ represent relative positions of neighboring j-th node of a segmented fiber with respect to the i-th node of the fiber in configurations Ω_0 and Ω_1, respectively, and are expressed as

$$\Delta\boldsymbol{X}_{ij} = \boldsymbol{X}_j - \boldsymbol{X}_i, \ \Delta\boldsymbol{x}_{ij} = \boldsymbol{x}_j - \boldsymbol{x}_i. \tag{S4-24}$$

When there is a unique linear mapping that transforms $\Delta\boldsymbol{X}_{ij}$ to $\Delta\boldsymbol{x}_{ij}$, $\Delta\boldsymbol{x}_{ij}$ can be expressed as

$$\Delta\boldsymbol{x}_{ij} = \boldsymbol{F}_i \cdot \Delta\boldsymbol{X}_{ij} \tag{S4-25}$$

where $\boldsymbol{F}_i$ is the deformation gradient at the *i*-th node. To compute optimal discrete deformation gradient at the *i*-th node, mapping error between fiber nodes *i* and *j* as the l_2 norm of the difference between $\Delta \boldsymbol{x}_{ij}$ and $\tilde{\boldsymbol{F}}_i \cdot \Delta \boldsymbol{X}_{ij}$ is defined by

$$\phi_{ij} = \left(\Delta \boldsymbol{x}_{ij} - \tilde{\boldsymbol{F}}_i \cdot \Delta \boldsymbol{X}_{ij}\right)^T \left(\Delta \boldsymbol{x}_{ij} - \tilde{\boldsymbol{F}}_i \cdot \Delta \boldsymbol{X}_{ij}\right) \tag{S4-26}$$

where $\tilde{\boldsymbol{F}}_i$ is the optimal discrete deformation gradient at the *i*-th node. Considering the weighted least square error among all of neighboring nodes of the *i*-th node, and summed weighted least square error at the *i*-th node is expressed as

$$\phi_i = \sum_{j=1}^{N} \phi_{ij} w_j = \sum_{j=1}^{N} \left(\Delta \boldsymbol{x}_{ij} - \tilde{\boldsymbol{F}}_i \cdot \Delta \boldsymbol{X}_{ij}\right)^T \left(\Delta \boldsymbol{x}_{ij} - \tilde{\boldsymbol{F}}_i \cdot \Delta \boldsymbol{X}_{ij}\right) w_j \tag{S4-27}$$

where w_j is a weight function (70), and w_j is given by

$$w_j(r) = \begin{cases} 1 - 6r^2 + 6r^3 : \ r \le \dfrac{1}{2}, \\ 2 - 6r + 6r^2 - 2r^3 : \ \dfrac{1}{2} < r < 1.0, \\ 0 : r \ge 1.0. \end{cases} \tag{S4-28}$$

where *r* is the distance of $\Delta \boldsymbol{x}_{ij}$, and normalized with cutoff length of 0.75 μm.

The optimal local discrete deformation gradient $\tilde{\boldsymbol{F}}_i$ is solved by minimizing ϕ_i with respect to nine components of $\tilde{\boldsymbol{F}}_i$. Thus, nine equations of $\dfrac{\partial \phi_i}{\partial \tilde{F}_{mn}} = 0$ for $1 \le m, n \le 3$ can be expressed as a tensor derivative:

$$\frac{\partial \phi_i}{\partial \tilde{\boldsymbol{F}}_i} = 2 \sum_{j=1}^{N} \left(\Delta \boldsymbol{x}_{ij} - \tilde{\boldsymbol{F}}_i \cdot \Delta \boldsymbol{X}_{ij}\right)^T \left(-\boldsymbol{I}_i \cdot \Delta \boldsymbol{X}_{ij}\right) w_j = 0 \tag{S4-29}$$

where $\boldsymbol{I}_i$ is the forth-order identity tensor, and the Equation (S4-29) becomes

$$\tilde{\boldsymbol{F}}_i \sum_{j=1}^{N} \left(\Delta \boldsymbol{X}_{ij}\right)^T \left(\boldsymbol{I}_i \cdot \Delta \boldsymbol{X}_{ij}\right) w_j = \sum_{j=1}^{N} \left(\Delta \boldsymbol{x}_{ij}\right)^T \left(\boldsymbol{I}_i \cdot \Delta \boldsymbol{X}_{ij}\right) w_j \tag{S4-30}$$

Since $\vec{a}\left(\boldsymbol{I}_i \cdot \vec{a}\right) = \vec{a} \otimes \vec{a}$, the Equation (S4-30) can be converted as

$$\tilde{\boldsymbol{F}}_i \sum_{j=1}^{N} \left(\Delta \boldsymbol{X}_{ij} \otimes \Delta \boldsymbol{X}_{ij}\right) w_j = \sum_{j=1}^{N} \left(\Delta \boldsymbol{x}_{ij} \otimes \Delta \boldsymbol{X}_{ij}\right) w_j . \tag{S4-31}$$

The above linear algebraic equations for the optimal discrete deformation gradient can be easily solved by inverting matrix $\sum_{j=1}^{N} \left(\Delta \boldsymbol{X}_{ij} \otimes \Delta \boldsymbol{X}_{ij}\right) w_j$ as

$$\tilde{\boldsymbol{F}}_i = \left(\sum_{j=1}^{N} \left(\Delta \boldsymbol{x}_{ij} \otimes \Delta \boldsymbol{X}_{ij}\right) w_j\right) \left(\sum_{j=1}^{N} \left(\Delta \boldsymbol{X}_{ij} \otimes \Delta \boldsymbol{X}_{ij}\right) w_j\right)^{-1} . \tag{S4-32}$$

Note, to avoid the singularity of matrix $\boldsymbol{A}$, at least three neighboring nodes at the *i*-th node are required and these neighboring nodes should be placed on the non-planar plane. Once $\tilde{\boldsymbol{F}}_i$ is obtained, the Lagrangian or Green strain tensor at the *i*-th node, $\tilde{\boldsymbol{E}}_i$, can be calculated using Eq. (S4-23):

$$\tilde{\boldsymbol{E}}_i = \frac{1}{2}\left(\tilde{\boldsymbol{F}}_i^T \tilde{\boldsymbol{F}}_i - \boldsymbol{I}\right). \tag{S4-33}$$

Text S1: Characterization of cell-probed stiffness

First, we aim to simulate mechanosensing tests for the two ECM fiber network models (Fig. S7A) in order to characterize and compare $\bar{E}^*$ and $\bar{k}_f^*$. Various simulations of mechanosensing tests for each ECM fiber network model were performed using a parameter of single fiber strain (Fig. S5 and S6). In both models of soft and stiff ECM, uniaxial tensile force was applied along two different direction in a cubic-shaped ECM fiber network model with a length of 20 μm for 15 s until each ECM model was strained up to 0.3 (Fig. S5A, and S6A). Afterwards, a single ECM fiber in the center of ECM fiber network model was forced to displace with the speed of a sinusoidal wave for 15 s, that is, single ECM fiber was tensioned during the first period of 7.5 s (from 15 to 22.5 s) and then was forced to relax during the second period of 7.5 s (from 22.5 to 30 s). Magnitudes of applied forces take maximum values at the time-point of 22.5 as the direction of the force is changed to the opposite direction (Fig. S5B, and S6B), and each graph of the rate of force with time has three saddle points since the second derivative of the force with respect to time is zero (Fig. S5C, and S6C). We find that both the CPSs using continuum mechanics (Fig. S7B) and the CPS using discrete fiber mechanics (Fig. S7C) are increased as single fiber strain increased in each ECM model, and two positive linear correlations between $\bar{E}^*$ and $\bar{k}_f^*$ (yellow marks i and ii in Fig. S5D and S6D), and one negative correlation (yellow mark iii in Fig. S5D and S6D). In particular, regions of positive linear correlations physically represent the force build-up (or protrusion) and the force drop-down (or retraction), respectively. The region of negative correlation is resulted from the fact that the second derivative of the force with respect to time is zero. Selected linear regressions at regions A and B in each ECM model show good correlations between $\bar{E}^*$ and $\bar{k}_f^*$ in the case of single fiber strain 0.3 (Fig. S5E, and S6E).

Second, we aim to simulate the mechanosensing of a cell interacting with the ECM of varying stiffness (Fig. S8). A computational model of ECM consisting of two distinct segments, soft and stiff, is constructed with two different pore sizes of 3.0 and 1.5 μm. Time-varying effective CPS was monitored at a filopodium (yellow circle marks in Fig. S8A and B). The effective CPS becomes higher as the filopodium starts interacting with stiffer ECM segment: a maximum value of effective CPS in Fig. S8C is ~10kPa, but a maximum value of effective CPS in Fig. S8D is ~30kPa. Furthermore, to justify our methods of calculating $\bar{E}^*$ and $\bar{k}_f^*$, these two kinds of effective CPSs were also compared at two different filopodial phases of protrusion (Fig. S9A) and retraction (Fig. S9B), respectively. Both methods of calculating effective CPSs show a good

agreement over two filopodial phases of protrusive and retraction. Statistical analysis of linear regression was performed by comparing both methods in terms of effective CPSs at the identical time-point. Good correlations were found between the two with R^2 = 0.801 and 0.890 for protrusive and retractile phases, respectively (Fig. S9C).

Supplementary References

1. Mogilner A, Rubinstein B (2008) The physics of filopodial protrusion. Biophys. J. 89: 782-795.
2. Lan Y, Papoian GA (2008) The stochastic dynamics of filopodial growth. Biophys. J. 94: 3839–3852.
3. Zhuravlev PI, Papoian GA (2009) Molecular noise of capping protein binding induces macroscopic instability in filopodial dyanamics. Proc. Natl Acad. Sci. USA 106: 11570–11575.
4. Bornschlögl T, Romero S, Vestergaard CL, Joanny JF, Van Nhieu GT, Bassereau P (2014) Filopodial retraction force is generated by cortical actin dyanamics and controlled by reversible tethering at the tip. Proc. Natl Acad. Sci. USA 110: 18928–18933.
5. Kim MC, Whisler J, Siberberg YR, Kamm RD, Asada HH (2015) Cell invasion dynamics into a three dimensional extracellular matrix fibre network. PLoS Comp Biol 11: e1004535.
6. Tsubota KI, Wada S, Yamaguchi T (2006) Particle method for computer simulation of red blood cell motion in blood flow. Computer Method and Programs in Biomedicine 83: 139–146.
7. Tsubota KI, Wada S (2010) Elastic force of red blood cell membrane during tank-treading motion: Consideration of the membrane's natural state. Int. J. of Mech. Sci. 52: 356–364.
8. Drury JL, Dembo M (2010) Aspiration of human neutrophils: Effects of shear thinning and cortical dissipation. Biophy. J. 81: 3166–3177.
9. Dembo M (1994) On peeling an adherent cell from a surface. In: Vol. 24 of series: Lectures on Mathematics in the Life Sciences, Some Mathematical problem in Biology. Providence: American Mathematical Society: 51–77.
10. Kanchanawong P, et al. (2010) Nanoscale architecture of integrin-based cell adhesions. Nature 468: 580–586.
11. Bell GI (1978) Models of specific adhesion of cells to cells. Science 200: 618–627.
12. Erdmann T, Schwarz UZ (2006) Bistability of cell-matrix adhesions resulting from nonlinear receptor-ligand dynamics. Biophys. J. 91: L60–L62.
13. Qian J, Wang J, Lin Y, Gao H (2009) Lifetime and strength of periodic bond clusters between elastic media under inclined loading. Biophys. J. 97: 2438–2445.
14. Hill AV (1938) The heat of shortening and the dynamic constants of muscle. Proc R. Soc. London B Biol. Sci. 126: 136–195.
15. Jeon J, Alexander NR, Weaver AM, Cummings PT (2008) Protrusion of a Virtual Model Lamellipodium by Actin Polymerization: A Coarse-grained Langevin Dynamics Model. J. Stat. Phys. 133: 79–100.
16. Kim MC, Kim C, Wood L, Neal D, Kamm RD, Asada HH (2012) Integrating focal adhesion dynamics, cytoskeleton remodeling, and actin motor activity for predicting cell migration on 3D curved surfaces of the extracellular matrix. Integ. Biol. (Camb) 4: 1386–1397.
17. Kim MC, Neal DM, Kamm RD, Asada HH (2013) Dynamic modeling of cell migration and spreading behaviors on fibronectin coated planar substrates and micropatterned geometries. PLoS Comp. Biol. 9: e100296.
18. Kabaso D, Shlomovitz R, Schloen K, Stradal T, Gov NS (2011) Theoretical model for cellular shapes driven by protrusive and adhesive forces. PLoS Comput. Biol. 7: e1001127.
19. Wang N, et al. (2002) Cell prestress. I. Stiffness and prestress are closely associated in adherent contractile cells. Am J. Physiol. Cell Physiol. 282: C606–C616.

20. Deguchi S, Ohashi T, Sato M (2006) Tensile properties of single stress fibers isolated from cultured vascular smooth muscle cells. J. Biomech. 39: 2603–2610.
21. Lu L, Oswald SJ, Ngu H, Yin FCP (2008) Mechanical Properties of Actin Stress Fibers in Living Cells. Biophys. J. 95: 6060–6071.
22. Walcott S, Sun SX (2010) A mechanical model of actin stress fiber formation and substrate elasticity sensing in adherent cells. Proc Natl. Acad. Sci. USA 107: 7757–7762 .
23. Zeng Y, Yip AK, Teo SK, Chiam KH (2012) A three-dimensional random network model of the cytoskeleton and its role in mechanotransduction and nucleus deformation. Biomech. Model Mechanobiol. 11: 49–59.
24. Stein AM, Vader DA, Weitz DA, Sander LM (2011) The micromechanics of three-dimensional collagen-I gels. Complexity 16: 22–28.
25. Yang Y, et al. (2008) Mechanical properties of native and cross-linked type i collagen fibrils. Biophys. J. 94: 2204–2211.
26. Deakin NE, Chaplain MAJ (2013) Mathematical modeling of cancer invasion: the role of membrane-bound matrix metalloproteinases. Frontiers in Oncology 3: 1–9.
27. C. J. Kim (2000) A coordinate-free form of the finite gradient in discretizing scalar and momentum diffusion. In proceedings of the 4th JSME-KSME Thermal Engineering Conference, Kobe, Japan.
28. Poincloux R, Lizárraga F, Chavrier P (2009) Matrix invasion by tumour cells: a focus on MT1-MMP trafficking to invadopodia. J. Cell Sci. 122: 3015–3024.
29. Abeyaratne R (2006) Lecture Note on the Mechanics of Elastic Solid. Volume I: A Brief Review of Some Mathematical Preliminaries. Department of Mechanical Engineering, MIT.
30. Gullett PM, Horstemeyer MF, Baskes MI, Fang H (2008) A deformation gradient tensor and strain tensors for atomistic simulations. Modelling Simul. Mater Sci. Eng. 16: 015001.